Title

The behavior of chalcophile elements during magmatic differentiation as observed in Kilauea Iki lava lake, Hawaii

Authors

Greaney, Allison T
Rudnick, Roberta L
Helz, Rosalind T
et al.

Publication Date

2017-08-01

DOI

10.1016/j.gca.2017.04.033

Peer reviewed

Available online at www.sciencedirect.com

ScienceDirect

Geochimica et Cosmochimica Acta 210 (2017) 71–96

Geochimica et Cosmochimica Acta

www.elsevier.com/locate/gca

The behavior of chalcophile elements during magmatic differentiation as observed in Kilauea Iki lava lake, Hawaii

Allison T. Greaney [a,*,1], Roberta L. Rudnick [a,1], Rosalind T. Helz [b], Richard M. Gaschnig [a,2], Philip M. Piccoli [a], Richard D. Ash [a]

[a] *University of Maryland – College Park, Department of Geology, College Park, MD 20742, USA*
[b] *United States Geological Survey, MS 926A, Reston, VA 20192, USA*

Received 27 July 2016; accepted in revised form 20 April 2017; Available online 27 April 2017

Abstract

We quantify the behavior of Cu, Ga, Ge, As, Mo, Ag, Cd, In, Sn, Sb, W, Tl, Pb, and Bi during the differentiation of a picritic magma in the Kilauea Iki lava lake, Hawaii, using whole rock and glass differentiation trends, as well as partition coefficients in Cu-rich sulfide blebs and minerals. Such data allow us to constrain the partitioning behavior of these elements between sulfide and silicate melts, as well as the chalcophile element characteristics of the mantle source of the Kilauea lavas. Nearly all of the elements are generally incompatible on a whole-rock scale, with concentrations increasing exponentially below ~6 wt% MgO. However, in-situ laser ablation data reveal that Cu, Ag, Bi, Cd, In, Pb, and Sn are chalcophile; As, Ge, Sb, and Tl are weakly chalcophile to lithophile; and Mo, Ga, and W are lithophile. The average $D^{\text{sulfide/silicate melt}}$ values are: $D_{Ag} = 1252 \pm 1201$ (2SD), $D_{Bi} = 663 \pm 576$, $D_{Cd} = 380 \pm 566$, $D_{In} = 40 \pm 34$, $D_{Pb} = 34 \pm 18$, $D_{Sn} = 5.3 \pm 3.6$, $D_{As} = 2.4 \pm 7.6$, $D_{Ge} = 1.6 \pm 1.4$, $D_{Sb} = 1.3 \pm 1.5$, $D_{Tl} = 1.1 \pm 1.7$, $D_{Mo} = 0.56 \pm 0.6$, $D_{Ga} = 0.10 \pm 0.3$, and $D_{W} = 0.11 \pm 0.1$. These findings are consistent with experimental partitioning studies and observations of Ni-rich sulfide liquid in mid-ocean ridge basalts (MORB), despite the different compositions of the KI sulfides. The KI glasses and whole rocks are enriched in As, Ag, Sb, W, and Bi, relative to elements of similar compatibility (as established by abundances in MORB), mimicking enrichments found in basalts from the Manus back arc basin (Jenner et al., 2012) and the upper continental crust (UCC). These enrichments suggest the presence of terrigenous sediments in the Kilauea mantle source. The KI source is calculated to be a mixture of depleted MORB mantle (DMM) and 10–20% recycled crust composed of MORB and minor terrigenous sediments.

Keywords: Chalcophile element; Partitioning; Differentiation; Kilauea Iki lava lake; Molybdenum

1. INTRODUCTION

Elements can be categorized into four major groups according to their geochemical behavior: lithophile (rock/silicate-loving), siderophile (iron-loving), chalcophile (sulfur-loving), and atmophile (gas-loving) (Goldschmidt, 1937). These classifications offer only the broadest descriptions of the behavior of an element, as composition

* Corresponding author.
E-mail address: greaney@umail.ucsb.edu (A.T. Greaney).
[1] Present address: University of California – Santa Barbara, Department of Earth Science, Santa Barbara, CA 93106, USA.
[2] Present address: University of Massachusetts – Lowell, Department of Environmental, Earth, and Atmospheric Science, Lowell, MA 01854, USA.

http://dx.doi.org/10.1016/j.gca.2017.04.033
0016-7037/

(including oxygen and sulfur fugacity), temperature, and pressure all affect the partitioning of elements in a given environment. The elements Cu, Ga, Ge, As, Mo, Ag, Cd, In, Sn, Tl, Pb, and Bi may be considered nominally chalcophile, as they form or preferentially partition into sulfides in surface environments (e.g., sedimentary basins, low T hydrothermal and epithermal systems), however their behavior in the core, mantle, and crust can vary quite dramatically. Elements like Cu and Ag behave as chalcophile elements in nearly all studied crystallizing environments. The remaining elements Ga, Ge, As, Mo, Cd, In, Sn, Sb, Tl, Pb, and Bi have been observed to either behave as structural components in sulfide phases (e.g., molybdenite MoS_2, galena PbS, stibnite Sb_2S_3, bismuthinite Bi_2S_3) or may substitute for the metal cation or anion (e.g., Ga, Ge, Cd and In replace Zn in sphalerite, ZnS). Their behavior in igneous systems, where magmatic sulfides crystallize or form immiscible liquids may be different, however, because element solubility as a cation or anion into a sulfide liquid can vary dramatically from its partitioning into a crystalline phase (Helmy et al., 2010). Many of these elements have been classified as lithophile elements in the bulk silicate Earth (e.g., Ga, Ge, Mo, In, Sn, Sb, Pb: Kuroda and Sandell, 1954; Yi et al., 2000; Jochum and Hofmann, 1997). Tungsten is generally considered to be moderately siderophile (Walker, 2016), but it is included in this study given its geochemical similarity to Mo.

A primary motivation for our study is to understand the partitioning behavior of Mo during igneous differentiation. Molybdenum is considered to be moderately siderophile during core formation (Walker, 2016), but is also found in the mantle, making it partially lithophile (Newsom and Palme, 1984). Molybdenum can also be chalcophile in low-temperature hydrothermal or sedimentary environments where it is concentrated in the ore mineral molybdenite and into syngenetic or diagenetic Mo-Fe-S phases formed in euxinic waters (Erickson and Helz, 2000; Helz et al., 2011; Gregory et al., 2015). Molybdenite is occasionally present as an accessory phase in rhyolite (Audétat et al., 2011). This variable behavior is driven by redox reactions. Molybdenum has garnered special interest because it is one of the most important tracers of atmospheric oxygen in the Precambrian due to its unique weathering properties that are dependent on its redox state – Mo is insoluble in the tetravalent state but it is soluble when oxidized to its hexavalent state. Therefore, Mo is thought to remain reduced, insoluble, and thus sequestered in the Archean crust before the 2.4 Ga Great Oxidation Event (GOE). Once the atmosphere became oxygenated, however, it is suggested that Mo was released from sulfides or other phases, oxidized to its soluble state, and washed into the oceans where it is concentrated in black shales. The Mo abundance in black shales has been one of the key observations used to determine exactly when O_2 rose in the atmosphere (Anbar et al., 2007; Scott et al., 2008). Thus, one of our aims is to test the hypothesis that Mo is primarily hosted in sulfides that will break down in the presence of atmospheric oxygen to release Mo. Because the Archean continental crust was likely significantly more mafic than the present-day crust (Taylor and McLennan, 1985; Condie, 1993; Tang et al., 2016; Gaschnig et al., 2016), studying Mo concentrations in sulfides blebs and other basaltic minerals provides a first-order approximation of the Mo distribution in Archean basalts and their differentiates that would have been weathered during the GOE.

A second motivation for this study is to use chalcophile element concentrations to gain insight into igneous petrogenesis and the nature of the Kilauea mantle source. Recent studies have provided better understanding of the formation of sulfides and the distribution and behavior of chalcophile elements during mantle melting and crust formation in MORB (Patten et al., 2013), arcs, and back arc basins (Jenner et al., 2010, 2012; Lee et al., 2012; Jenner et al., 2015) and. However, the behavior of many of these chalcophile elements during magmatic differentiation is less constrained, save for a few (e.g., Ga, Kato et al. (2017); Mo, Yang et al. (2015); Cd, In, and Sn, Yi et al. (2000) and Jochum et al. (1993); Sb, Jochum and Hofmann (1997); W, Arevalo and McDonough (2008); Tl, Prytulak et al. (2013), and Pb, Hofmann (1988)). In these element-specific studies, the mineralogical hosts were not empirically determined. Differentiation trends for these elements can be used to infer mantle source compositions. The nature of the mantle source of the Hawaiian hot-spot is debated, however many researchers argue for a depleted mantle source containing varying proportions of recycled oceanic crust, as initially proposed by White and Hofmann (1982). By documenting the behavior of variably chalcophile elements during differentiation in the Kilauea Iki lava lake, we can identify their mineralogical hosts and estimate the mantle source abundances, as done previously for platinum group elements (Puchtel et al., 2004) and W (Ireland et al., 2009), to gain insights into its formation.

We present data for Cu, Ga, Ge, As, Mo, Ag, Cd, In, Sn, Sb, W, Tl, Pb, and Bi in the Kilauea Iki lava lake. This includes whole rock analyses, in-situ mineral analyses, and determination of partition coefficients between the melt and sulfides, silicates, and oxides.

2. KILAUEA IKI LAVA LAKE

The Kilauea Iki lava lake formed when picritic lava ponded in a pre-existing crater during the 1959 eruption of Kilauea volcano. The lava was emplaced in seventeen eruptive phases over the course of four weeks (Richter and Moore, 1966), and subsequently cooled and differentiated as a closed system over the following decades, thus providing an excellent natural laboratory to study magmatic differentiation. The eruption was well documented and several drilling excursions from 1960 to 1988 have provided numerous cores that have been extensively analyzed. Data for major elements (Helz et al., 1994; Helz and Taggert, 2010), lithophile trace elements (Helz, 2012), highly siderophile trace elements (Pitcher et al., 2009), and numerous stable isotope systems (Tomascak et al., 1999; Teng et al., 2007, 2008; Chen et al., 2013; Savage et al., 2015) have been published.

The Kilauea Iki core samples are dominated by picrite and basalt, but also contain internal differentiates resulting from discontinuous fractionation processes (Helz, 1987).

The picrites and basalts range in whole rock (WR) MgO content from 27 wt% (olivine cumulates) to 7.5 wt% and contain varying proportions of olivine and chromite as well as occasional plagioclase, augite, and Fe-Ti oxides. The average composition of the lave lake is around 15 wt% MgO_{WR} (Wright, 1973). The majority of the internal differentiates are ferrodiabasic segregation veins (<6 wt% MgO_{WR}, up to 57 wt% SiO_{2WR}) that formed as evolved residual liquid segregated from the surrounding crystal mush by flowing into cracks created in the cooling lake. The segregation veins contain plagioclase, augite, Fe-Ti oxides, minor acicular apatite, an immiscible sulfide, and silicate glass that is quite felsic (between 56 and 74 wt% SiO_{2glass}), relative to most quenched basalts. Fe-Ni-Cu sulfide blebs were previously documented within melt inclusions hosted in olivine in the picrite and basalt samples (Stone and Fleet, 1991; Helz and Wright, 1992) and Cu-rich sulfide blebs have been previously documented in the groundmass of the more evolved samples (Helz, 1987; Stone and Fleet, 1991; Pitcher et al., 2009). Because parts of the lake were still molten during drilling, melt was quenched upon extraction, preserving glass in many samples. Glass quenching temperatures in drill cores range from ~1150 °C in the most mafic rocks to ~900 °C in the more evolved samples (Helz and Thornber, 1987), although most samples were completely cooled and solidified by the time they were drilled. Oxygen fugacities in the lake were determined using the oxide oxybarometer of Ghiorso and Evans (2008) and evolve from ΔNNO+1.5 to ΔNNO−1, which corresponds to different stages of crystallization (supplementary figures). A complete thermal history of the lake from the 1981 drill-core is documented in Helz and Thornber (1987).

Thirty-six samples ranging from 26.9 to 2.4 wt% MgO_{WR} (Table 1) were analyzed for whole rock and/or in-situ chalcophile element data. Samples were chosen based on previous characterization, MgO content, thermal history, and mineralogy. The modal mineralogy of select samples was determined by point counting and can be found in Table A7.

3. METHODS

3.1. Whole rock analyses

Twenty-one whole rock powders, four USGS standard reference materials (BHVO-1, W-2, AGV-2, and GSP-1), and a total analytical blank (TAB) were analyzed using standard addition solution inductively coupled mass spectrometry (ICP-MS) and externally calibrated solution ICP-MS. Fifty milligrams of powder were dissolved in Savillex beakers for the KI samples, BHVO-1, and W-2. High-pressure Teflon© Parr bombs were used to digest the more felsic standards (AGV-1 and GSP-1) to ensure dissolution of resistant phases. One mL of concentrated HNO_3 and 3 mL of concentrated HF were added to the beakers and bombs, which were then placed on a hotplate (150 °C) or in an oven (180 °C), respectively, for ≥72 h. The solutions were then evaporated to dryness on a hotplate and 2 mL of concentrated HNO_3 were added and subsequently evaporated before adding 1 mL of HNO_3 and 2 mL of 18 Ω MilliQ H_2O, resealing the beakers/bombs, and replacing them on the hotplate/furnace overnight (≥12 h). The beakers/bombs were removed the next day and "master solutions" were made, consisting of the dissolved solution (sample + 1 mL of HNO_3 + 2 mL of MilliQ H_2O) diluted to 15 mL with 2% HNO_3 and trace HF. Sample dissolution and standard addition procedures follow the procedures of Gaschnig et al. (2015).

The standard addition technique involves spiking the solution of unknown concentration with known concentrations of the element of interest, and using the spiked samples to create a calibration curve. Two spikes were prepared: Spike A contains Ag, Cd, In, Sb, Tl, and Bi and Spike B contains Ga, Ge, Sn, Mo, and W. For the most accurate results, the spikes were prepared so that they contain roughly double the concentration expected in the samples. Three solutions were created for each sample + spike combination. Solution one contains 1 mL of master solution and 1 mL of a purified Rh solution in 2% HNO_3 (~75 ppb) to be used as a drift corrector. Solution two contains 1 mL of master solution, 1 mL of Rh, and 0.5 mL of spike. Solution three contains 1 mL of master solution, 1 mL of Rh, and 1 mL of spike. The three aliquots were diluted to a total volume of 10 mL with 2% HNO_3 then vigorously shaken to homogenize the solution.

Additionally, a separate 1 mL aliquot of the master solution was spiked with 1 mL of ~800 ppb In (drift corrector) and diluted to 15 mL with 2% HNO_3 for Cu, Pb and other trace element analyses. These data were reduced with an external calibration curve created with the USGS standards. The standard addition and In-spiked solutions were run on a Thermo-Finnigan Element2 HR-ICP-MS at the University of Maryland within a week of solution preparation. The instrument was tuned to keep oxide production below 0.8% $^{238}U^{16}O/^{238}U$. Multiple isotopes of most elements were run in low (LR) and some were run in medium (MR) resolution to reduce polyatomic and isobaric interferences. For the suite of chalcophile elements, the following isotopes were measured: ^{69}Ga (MR), ^{71}Ga (MR), ^{73}Ge (MR), ^{74}Ge (MR), ^{75}As (MR), ^{95}Mo (LR, MR), ^{97}Mo (LR, MR), ^{98}Mo (LR, MR), ^{107}Ag (LR, MR), ^{109}Ag (LR, MR), ^{111}Cd (LR, MR),^{115}In (LR, MR), ^{117}Sn (LR, MR), ^{118}Sn (LR, MR), ^{119}Sn (LR, MR), ^{121}Sb (LR, MR), ^{182}W (LR, MR), ^{183}W (LR, MR), ^{205}Tl (LR), and ^{209}Bi (LR). The ^{115}In data were corrected for interferences by ^{115}Sn (resulting in a 10% difference, on average). Copper-63, ^{65}Cu, ^{206}Pb, and ^{208}Pb were analyzed with the external calibration method. Precision was determined using replicate analyses of BHVO-1 and AGV-2 (Table A1 and supplementary figures). The standard addition data were reduced using an in-house Excel macro created by Ming Tang.

3.2. *In-situ* analyses

In-situ analyses of glass, silicates, oxides, and sulfide blebs were carried out on eighteen petrographic thin sections. The phases were analyzed for major element compositions using WDS on a JEOL JXA-8900 Electron Probe

Table 1
Sample descriptions.

Sample	Rock type	Analysis	MgO WR	MgO glass	Temp, °C	fO2, ΔNNO	Sulfides	Glass %
67-2-83.7	segregation vein	LA	*nd*	1.77	*1015*		none	2.9
67-3-70.0	ferrodiabase segregation vein	LA	*nd*	0.09	972		gmass	13
67-3-75.0	ferrodiabase segregation vein	LA	*9.47*	0.51	990		gmass	11
67-3-75.7	ferrodiabase segregation vein	LA	*nd*	0.49	1000	−0.57	gmass	32
67-3-76.2	ferrodiabase segregation vein	LA	*5.14*	0.66	1015	−0.66	gmass	26
75-1-125.0	ferrodiabase segregation vein	LA	*5.94*	0.09	975	−0.91	gmass	25
75-1-130.5	Olivine basalt	LA	*9.73*	0.40	980	0.44	gmass, incl	4.8
75-1-134.4/133.4	olivine basalt	LA, SA	*10.65*	2.01	1037		gmass	16
79-1R1-170.9	ooze from segregation vein	LA, SA	*3.48*	1.78	*110*		gmass	58
79-3-150.4	olivine basalt	LA, SA	*13.51*	no glass	*825*		gmass, incl	0
79-3-158.0	ferrodiabase segregation vein	LA, SA	*4.5*	0.37	*990*	−0.45	gmass	17
79-3-160.6/160.3	olivine basalt	LA, SA	*16.11*	0.61	*110*	1.53	inclusion	9.0
79-3-171.9/172.8	olivine basalt	LA, SA	*18.8*	4.32	*110*	1.38	none	29
81-2-88.6	vein within a segregation vein	LA, SA	*2.37*	no glass	*110*	-0.89	gmass	0
81-1-169.9	segregation vein, olivine rich	LA	*nd*	0.14	970		gmass	5.2
81-1-178.9b	olivine basalt	LA	*nd*	0.79	995		gmass	7.8
81-1-178.9sv	ferrodiabase segregation vein	LA	*nd*	0.52	995		gmass	23
81-1-210.0/209.8	olivine basalt	LA, SA	*24.53*	6.09	*1135*		none	18
81-1-294.7	olivine basalt	LA, SA	*14.3*	5.03	1105		none	24
Iki 58	eruption pumice	SA	*8.08*	*nd*	*1144*		*nd*	*nd*
Iki 22	eruption pumice	SA	*19.52*	*nd*	*1216*		*nd*	*nd*
Iki 3	eruption pumice	SA	*17.2*	*nd*	*1213*		*nd*	*nd*
67-2-85.7	ooze from segregation vein	SA	*2.6*	*nd*	*1060*		*nd*	*nd*
67-3-6.8	chilled upper crust	SA	*25.83*	*nd*	*110*		*nd*	*nd*
67-3-27.5	chilled upper crust	SA	*12.01*	*nd*	*110*		*nd*	*nd*
75-1-38.9	chilled upper crust	SA	*10.73*	*nd*	110		*nd*	*nd*
75-1-75.2	ferrodiabase segregation vein	SA	*5.77*	*nd*	110		*nd*	*nd*
75-1-121.5	olivine poor basalt	SA	*7.77*	*nd*	*850*		*nd*	*nd*
81-1-119.2	olivine basalt	SA	*6.74*	*nd*	*110*		*nd*	*nd*
81-1-169.9x	basalt from olivine diapir	SA	*26.87*	*nd*	*975*		*nd*	*nd*
81-1-239.9	olivine basalt	SA	*26.55*	*6.13*	*1140*		*nd*	*nd*

*SA = standard addition (whole rock) and LA = laser ablation (of glass).
*WR data is from Helz and Taggert (2010).
*Temperatures were calculated from equations in Helz and Thornber (1987), italics note temperatures calculated by Roz Helz. fO2 calculated from Ghiorso and Evans (2008).
*gmass = groundmass sulfides, incl = olivine-hosted melt inclusion sulfides.
*nd = not determined, used for samples that were only analyzed by one method (SA or LA) and thus other data is missing.

Micro Analyzer (EPMA) at the University of Maryland. Between 8 and 10 points were measured on glass per sample and a mean was calculated for each sample showing homogeneous glass composition (all glasses were homogeneous except for 67-3-83.7 and 75-1-130.5, which contain less than 5% glass). A total of ~245 EPMA point analyses were made on ~190 sulfides from 13 thin sections. At least two points were analyzed on sulfides that were larger than 10 μm to check for compositional heterogeneity due to exsolution. Many sulfides showed multiple regions of heterogeneous exsolution, making it nearly impossible to extrapolate the data collected from a 2-dimensional cross section of the sulfide sphere to what may lie below or above the plane of the thin section. Therefore, the true major element composition of the sulfide blebs is uncertain. Such heterogeneity was taken into consideration when reducing the laser ablation (LA) ICP-MS data. All EPMA analyses were performed with a 5 μm beam, 15 kV accelerating voltage, and 25 nA probe current.

Trace element abundances were determined using LA-ICP-MS at the University of Maryland. The phases were ablated in a He atmosphere using a New Wave UP 213 nm wavelength laser and the resulting sample plume was analyzed with a Thermo-Finnigan Element2 HR-ICP-MS. The instrument was tuned so that the $^{238}U^{16}O/^{238}U$ ratio was below 0.8%. All substrates were ablated with a laser frequency of 7 Hz and fluence was kept between 2.5 and 4 J/cm^2, depending on the substrate being analyzed. The isotopes measured were: ^{63}Cu, ^{65}Cu, ^{69}Ga, ^{71}Ga, ^{73}Ge, ^{74}Ge, ^{75}As, ^{95}Mo, ^{97}Mo, ^{98}Mo, ^{107}Ag, ^{109}Ag, ^{111}Cd, ^{113}In, ^{115}In, ^{117}Sn, ^{119}Sn, ^{121}Sb, ^{123}Sb, ^{184}W, ^{205}Tl, ^{208}Pb, and ^{209}Bi. The In data were corrected for interferences by ^{113}Cd and ^{115}Sn. Glass, silicate, and oxide analyses were performed using a laser spot size between 55–80 μm, and sulfide analyses were performed with a spot size of 25–80 μm, depending on the size of the phase being ablated. Between 6 and 10 glass points were measured per thin section and then averaged for a sample mean. Samples that contain heterogeneous glasses were not used in *D* value calculations. Thirty-two sulfides (>25 μm) within six thin sections were ablated, but because of the small size of the sulfide blebs it was not possible to ablate distinct unmixed

regions within a bleb. Data reduction for LA-ICP-MS was performed using NIST 610 as the external calibration standard and the Iolite software created at the University of Melbourne (Paton et al., 2011). Silicon was used as an internal standard for silicate phases, Cu for sulfides, and Mn for oxides. Only sulfides that were in contact with homogeneous glass were targeted for LA-ICP-MS analysis. Because several sulfides have heterogeneous major element abundances, the raw sulfide ablation data was reduced twice: once using the highest Cu content measured by EPMA and once using the lowest Cu content. Of the 32 sulfides ablated, only five were compositionally heterogeneous enough to yield two reduction values that varied by more than 10%. The two reduction values for the 27 homogeneous sulfides were then averaged to give a single concentration for each trace element in each sulfide. For example, two distinct unmixed regions of a sulfide may contain 42 wt% and 50 wt% Cu each, so the resulting ablation data was reduced once using the 42 wt% Cu endmember and a then re-reduced using the 50 wt% Cu end member. These two reduction schemes gave two separate endmember values for the trace elements of interest, which were then averaged if they varied by less than 10%. Reference materials BHVO-2g, NIST-612, and JB sulfide (a reference sulfide created by James Brenan at the University of Toronto, Mungall and Brenan, 2014) were used as secondary standards during laser ablation analyses. Values determined for standard reference materials are provided in Table A1.

4. SULFIDES

4.1. Sulfide textures and composition

Visible sulfides in the samples form round droplets between one and 200 μm in diameter. These immiscible sulfide phases are common in basaltic melts and are often referred to as "blebs" as they are near-spherical in shape. Within the lake, the sulfides are found in the groundmass of the most evolved basalts and segregation veins, and occasionally within melt inclusions in olivine phenocrysts of the more primitive samples. Here we focus on the groundmass sulfides in the most evolved samples with quite felsic (nearly rhyolitic) glass, as opposed to other studies (Patten et al., 2013) where sulfides blebs were in contact with basalt glass.

In reflected light, most sulfides appear to be composed of a yellow[3], relatively Cu-poor phase and an orange, Cu-rich phase. However, the exact abundance of Cu, Fe, and S in these exsolved regions varies from sulfide to sulfide. Native Cu is observed in several sulfides (Fig. 1a), and rare Fe-oxides are found as inclusions within some blebs. Exsolution textures range from simple to complex, including very fine-grained, acicular lamellae, and massive exsolution features, as shown in Fig. 1. The groundmass sulfide blebs are all Cu-Fe-S phases that form a solid solution between isocubanite, $CuFe_2S_3$, and bornite, Cu_5FeS_4 (Fig. 2) with rare Ni present. Complete major and trace element data for the sulfides can be found in Table A6.

[3] For interpretation of color in Fig. 1, the reader is referred to the web version of this article.

The blebs likely represent immiscible sulfide melt droplets that unmixed following quenching to subsolidus temperatures, with crystallization towards bornite and isocubanite endmembers. The textures of sulfide blebs suggest sulfide liquid immiscibility and the Cu-rich composition is likely reflective of formation by in-situ crystallization in an evolved, Cu-rich melt. In samples with abundant glass, roughly half of the sulfides are surrounded by glass while the other half appear to have nucleated onto another phase (typically Fe-Ti oxides, Fig. 1a, b, c). In samples with minor glass (<8 vol%), sulfides are found as interstitial phases sandwiched between olivine, augite, and plagioclase (Fig. 1d). A complete list of sulfide textures, size, and composition is provided in Table A6.

The sulfides that are found in the eruption sample Iki-22 and within melt inclusions in olivine phenocrysts are compositionally distinct from the groundmass sulfides in the evolved samples, as they contain significantly more Ni. Up to 11 wt% Ni was measured in this study, however a previous study found up to 31 wt% in the sulfide blebs in Iki-22 which were determined to be either pentlandite or MSS (Stone and Fleet, 1991).

4.2. Sulfide equilibrium

In order for partition coefficients to be valid, the sulfides must be in equilibrium with the glass, and the glass must be homogenous. While equilibrium can be difficult to establish in natural systems, sulfide-glass equilibrium can be evaluated in the KI samples from the following criteria set by Peach et al. (1990) and Li and Audétat (2015), and this study: (1) there is no correlation between sulfide size and composition; (2) the sulfides are compositionally homogeneous; and (3) the sulfides are in direct contact with the glass. The first requisite is met, as there is no correlation observed between sulfide diameter and major or trace element composition. This implies that the surrounding silicate melt did not significantly change in composition during sulfide growth as would be the case if larger (older) sulfides were enriched in silicate-incompatible chalcophile elements compared with the smaller (younger) sulfides. This also suggests that the surrounding melt was not chemically isolated (i.e., interstitial) during sulfide growth. The second criterion is difficult to evaluate given the exsolved nature of the sulfides, but they all form Cu-Fe-S solid solutions between isocubanite and bornite, and the Cu content of all sulfides in the same thin section varies by less than 30%. Finally, while many occurrences of sulfides are found throughout the KI samples, only those in direct contact with glass were analyzed using LA-ICP-MS (see Fig. 1a, b, c). All of these samples have greater than 15% glass by volume, with the exception of one (sample 81-1-169.9, which is at a higher risk for disequilibrium). It can thus be inferred that the melt was interconnected and grain boundaries were likely wetted in these glassy samples, implying sulfides were in direct contact with the melt until the molten rock was quenched (Miller et al., 2014). Additionally, only samples with relatively homogeneous glass were used in D value calculation where the 2 sigma RSD calculated on multiple point analyses of glasses was less

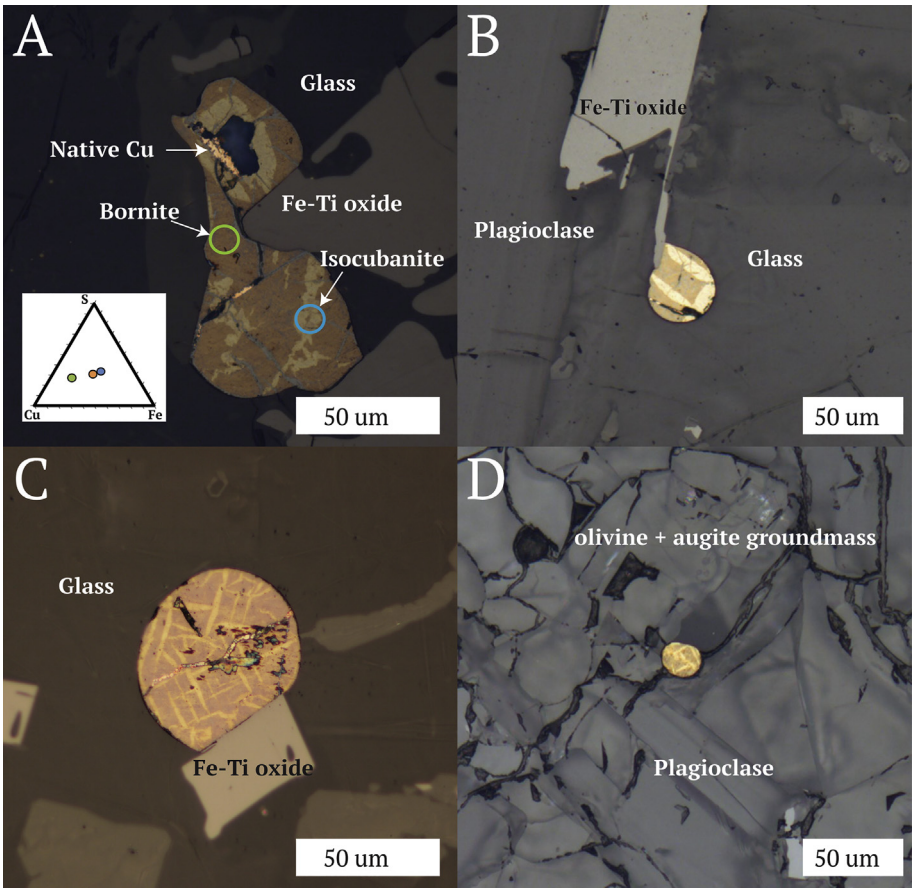

Fig. 1. Photomicrographs of typical sulfides found in the KI groundmass. (A) An irregular shaped sulfide with complex exsolution textures. Four points measured with EPMA display four distinct phases: chalcopyrite, bornite, isocubanite, and native Cu. Normalized EPMA analyses are shown on the inset ternary diagram. (B) "Simple" massive exsolution texture on a sulfide that likely nucleated onto an Fe-Ti oxide. (C) Lamellar/acicular exsolution texture. (D) An interstitial sulfide found in a sample with minor glass. The sulfide still retains its rounded shape and displays exsolution lamellae. Interstitial sulfides like this were not analyzed using laser ablation ICP-MS because they are not in direct contact with glass. All photos taken in reflected light.

than 25% for all elements except Ag, Cd, In, Sb, and Bi (the least abundant elements in the glasses, so their large RSD is a function of difficulty measuring ppb-level abundances with LA-ICP-MS). In summary, although caution should be taken when claiming true equilibrium in a crystallizing system, the criteria above suggests the sulfides equilibrated with the evolved, intermediate silicate melt. Thus, this study provides an assessment of partitioning behavior in a natural system.

5. RESULTS

5.1. Whole rock differentiation trends

In the whole rocks, all elements (except for Ge) become more concentrated with increasing differentiation (Fig. 3, Table 2). Because the concentrations of many of the elements of interest increase nearly exponentially with decreasing MgO content, it can be inferred that they behave incompatibly on a whole rock scale during differentiation of the lava lake. By contrast, Ge maintains a relatively constant concentration in all of the Kilauea samples.

The erupted pumice samples Iki-3 (17.2 wt% MgO_{WR}) and Iki-22 (19.5 wt% MgO_{WR}) show anomalous enrichments in several elements (Sn, Pb, Mo, Bi, Cd, Sb) that cannot be explained given the observed mineralogy of the samples in thin sections. Similar anomalous enrichments were found in KI eruption pumice and basalt analyzed by Pitcher et al. (2009) where spikes in some PGEs (especially Pt in Iki-22 and Ru and Ir in the glass separate, Iki-22g) were attributed to precipitation of metal or alloy "micronuggets" that were not visible in thin section but may impart a "nugget effect" on the whole rock data. The origin of these enrichments is further discussed in Section 6.1.

5.2. Glass analyses

While the chalcophile elements appear to behave incompatibly on a whole rock scale, glass analyses better reflect the partitioning of several elements due to the saturation and/or fractionation of various phases. Variation diagrams of the glass trace element analyses are displayed in Fig. 4 and the data can be found in Table 3. The most primitive glass measured in this study contains 6.1 wt% MgO. The

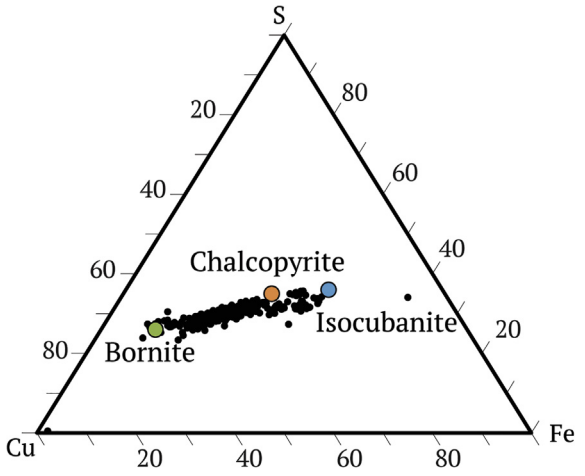

Fig. 2. Ternary diagram of ~245 EPMA point analyses measured on ~180 sulfides. The green symbol represents bornite, the orange chalcopyrite, and the blue is isocubanite, showing that the KI sulfide blebs found within the glass form a solid solution between the bornite and isocubanite endmembers. (For interpretation of the references to color in this figure legend, the reader is referred to the web version of this article.)

average MgO content of the parental erupted melt was between 8.5 and 9.0 wt% as determined by scoria glasses (Helz et al., 2017). The majority of the glasses analyzed here are from segregation veins where the glass is actually quite felsic (between 0.2 and 3.0 wt% MgO_{glass}), as these are the samples where sulfide is most easily found.

We have demonstrated the highly chalcophile nature of Cu in this system, hence we can use it as a proxy for S since the latter is compromised by degassing during eruption and drilling (Helz and Wright, 1983). Copper abundance in the glass steadily increases from 6 to 2 wt% MgO_{glass} and then abruptly falls, consistent with sulfide saturation at around 2 wt% MgO_{glass} (Fig. 4). Because the melt saturates with respect to sulfides, but sulfide droplets do not physically segregate from the magma, these decreases in abundances are not observed in the whole rock data. Other chalcophile elements that show a drop in overall abundance below 2 wt % MgO_{glass} are Ag, Cd, In, and Bi.

Arsenic, Ga, and Ge appear to decrease in abundance at around 1 wt% MgO. The abundances of Mo, Sn, Sb, W, Tl, and Pb in the glass all increase, to varying degrees, with increasing differentiation, suggesting that these elements behave relatively incompatibly in the system and they are not significantly influenced by sulfide formation. This is further supported by an inverse relationship between the glass abundance of a sample and the concentrations of elements Mo, Sn, Sb, W, and Tl, suggesting they are strongly concentrated into the last vestiges of melt.

5.3. Partition coefficients

Partition coefficients (D values) and chalcophile element abundances for the sulfides are presented in Tables 4 and 5, and D values for other oxides and silicates can be found in Tables 6 and 7, respectively. Partition coefficients were calculated as C^{phase}/C^{glass} using the mean glass composition for a given sample.

5.3.1. Sulfides

Partition coefficients were calculated for each sulfide in a thin section (between 1 and 9 per section) by taking the mean sulfide composition divided by the mean glass composition for the sample. Taking the mean of the $D^{sulfide/silicate}$ values for the five samples measured gives $D_{Ag} = 1252 \pm 1201$ (2σ), $D_{Bi} = 663 \pm 576$, $D_{Cd} = 380 \pm 566$, $D_{In} = 40 \pm 34$, $D_{Pb} = 34 \pm 18$, $D_{Sn} = 5.3 \pm 3.6$, $D_{As} = 2.4 \pm 7.6$, $D_{Ge} = 1.6 \pm 1.4$, $D_{Sb} = 1.3 \pm 1.5$, $D_{Tl} = 1.1 \pm 1.7$, $D_{Mo} = 0.56 \pm 0.6$, $D_{Ga} = 0.10 \pm 0.3$, and $D_W = 0.11 \pm 0.1$. The partition coefficients span nearly six orders of magnitude between the elements of interest (Fig. 5), so they are divided up into three categories: (1) chalcophile elements, average $D \geq 5$: Ag, Bi, Cd, In, Pb, and Sn; (2) weakly chalcophile elements, average $D \sim 1$: As, Ge, Sb, and Tl; and (3) non-chalcophile elements, $D < 1$: Mo, Ga and W. Within the chalcophile elements, subgroups could be created for strongly chalcophile (Ag, Bi, Cd, In) and chalcophile (Pb and Sn) elements. This is because Pb and Sn do not decrease in abundance in the glasses after sulfide saturation, showing that sulfide saturation does not completely control their behavior. Partition coefficients are not plotted for Cu because it is an essential structural constituent of the sulfides, ranging between 25 and 58 wt%; D_{Cu} can reach up to 19,000.

5.3.2. Oxides

The crystallizing oxides (pseudobrookite and ilmenite) contain minor amounts of Cu, Ga, Mo, Ag, Cd, and In and have partition coefficients ($D^{oxide/silicate\ melt}$) greater than or equal to one, so the oxides can be considered as minor-mineralogical hosts (Table 6, chalcophile element abundances in Table A4). Ilmenite contains Ag ($D \sim 4$), Cd ($D \sim 1$), and In ($D \sim 3$). Pseudobrookite contains Cu ($D \sim 1$), Ga ($D \sim 1$), Mo ($D \sim 1$), Ag ($D \sim 3$), Cd ($D \sim 1$), and In ($D \sim 2$). Oxide fractionation does not significantly deplete these elements in the melt, as there is no decrease in overall abundance below ~5 wt% MgO_{glass} (Fig. 4).

5.3.3. Silicates

Olivine and augite are the only two silicates analyzed in this study, but neither are significant hosts of the elements investigated here. The D values calculated for all of the elements are below one (Table 7, chalcophile element abundances in Table A5). Plagioclase was not analyzed, as it was not expected to be a significant host of any of these elements with the exception of Ga and Ge, which may substitute for Al and Si, respectively.

6. DISCUSSION

6.1. Element volatility

Anomalous spikes of Mo, Cd, Sn, Sb, Pb, Bi in the whole rock data are present in two of the three eruption pumice samples and one of the eighteen drill core basalts

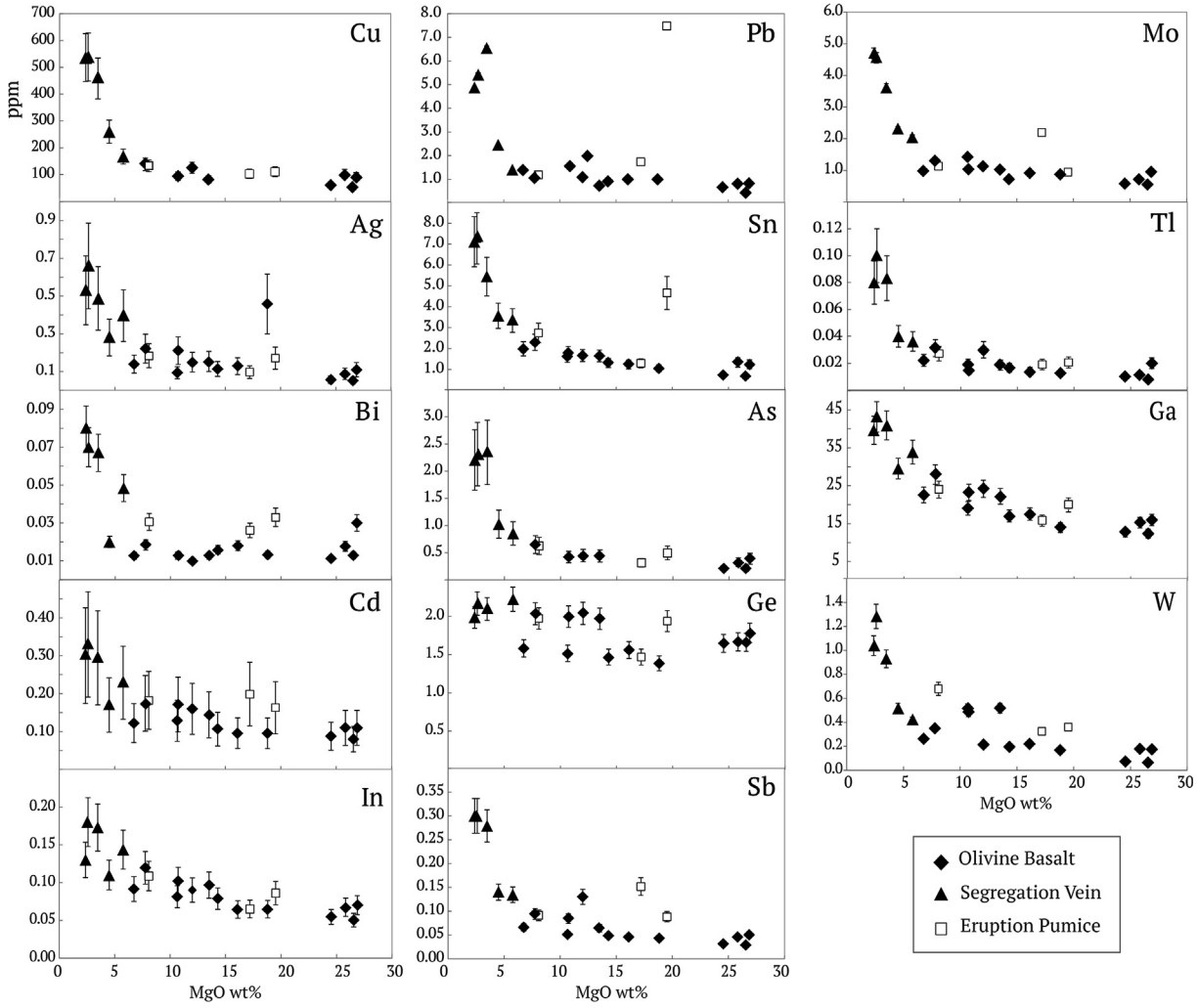

Fig. 3. MgO variation diagrams displaying chalcophile element differentiation trends in the whole rock powders. All trace elements are measured in ppm. Error bars denote 2SD as determined by replicate analyses of BHVO-1 (MgO = 7.2 wt%) and may be an overestimate for the segregation vein samples that are more enriched in the chalcophile elements.

(Fig. 3). Given that the enrichments are primarily concentrated in the eruption phases and similar anomalies are observed in the PGEs (Pitcher et al., 2009), we propose that some chalcophile elements and PGEs partition into a vapor phase during eruption and precipitated in condensates from this vapor.

Rhenium volatility during basaltic volcanism is well documented (Sun et al., 2003; Lassiter, 2003; Norman et al., 2004; Pitcher et al., 2009) and it has been suggested that vapor-phase Re is deposited in Re-sulfides (Korzhinsky et al., 1994) or Mo- and Bi-bearing phases in fumarolic fields (Tessalina et al., 2008). Enrichments in Cu, As, Sb, Te, Tl, and Pb have also been documented in condensed vapor from fumarole gas jets (Korzhinsky et al., 1994). Thus, vaporization during eruption and subsequent precipitation is a possible cause of the enrichments seen in the KI pumice.

The potential loss of volatile elements from the lava lake could decrease their concentrations in the glasses and whole rocks. For example, Yi et al. (2000) showed that subaerial outgassing lowers Cd abundances in basalts, and Norman et al. (2004) calculated that Cd outgassing, alongside Re and S, may lower Cd concentrations in volcanic glass by a factor of 2–5. Bismuth may also be slightly affected by this process, however, significant depletions of the volatile elements In, Sn, Cu and Pb due to outgassing is considered unlikely (Yi et al., 2000; Norman et al., 2004). To our knowledge, the influence of volatility on Mo and Sb concentrations in whole rock and glass has not been determined. We conclude that Mo, Cd, Sn, Sb, Pb, Bi may have partitioned into a vapor phase to varying degrees, however the extent of their possible depletion from the lava lake is unknown. The results of previous work on Cd and Bi outgassing prompt us to take caution when interpreting the absolute abundances of these elements in the KI magma.

6.2. Sulfide genesis and evolution

The Cu-rich groundmass-hosted sulfides in the Kilauea Iki drill core samples are compositionally distinct from

Table 2
Chalcophile element abundances (ppm) in whole rock powders. Complete major element and trace element data are presented in appendix Table A2.

	MgO wt%	Cu	Ga	Ge	As	Mo	Ag	Cd
Iki 58	**8.08**	**132**	**24.0**	**1.97**	**0.63**	**1.13**	**0.18**	**0.18**
2s		31.1	4.3	0.43	0.10	0.27	0.08	0.05
Iki 22	**19.5**	**111**	**19.9**	**1.94**	**0.50**	**0.94**	**0.17**	**0.16**
2s		27.6	3.6	0.42	0.08	0.22	0.08	0.04
Iki3	**17.2**	**103**	**15.8**	**1.47**	**0.32**	**2.19**	**0.10**	**0.20**
2s		3.40	2.8	0.32	0.05	0.52	0.04	0.05
81-2-88.6	**2.37**	**537**	**39.6**	**1.98**	**2.20**	**4.70**	**0.53**	**0.30**
2s		40.2	7.1	0.43	0.36	1.11	0.23	0.08
67-2-85.7	**2.72**	**539**	**43.2**	**2.17**	**2.31**	**4.55**	**0.66**	**0.33**
2s		40.5	7.8	0.47	0.38	1.07	0.29	0.08
79-1R1-170.9	**3.48**	**459**	**40.9**	**2.09**	**2.35**	**3.61**	**0.49**	**0.29**
2s		35.5	7.4	0.45	0.38	0.85	0.21	0.07
79-3-158.0	**4.50**	**260**	**29.5**	**1.70**	**1.03**	**2.30**	**0.28**	**0.17**
2s		20.3	5.3	0.37	0.17	0.54	0.12	0.04
75-1-75.2	**5.77**	**167**	**33.9**	**2.22**	**0.86**	**2.04**	**0.40**	**0.23**
2s		43.8	6.1	0.48	0.14	0.48	0.17	0.06
75-1-121.5	**7.77**	**139**	**27.9**	**2.03**	**0.65**	**1.33**	**0.22**	**0.17**
2s		33.5	5.0	0.44	0.11	0.31	0.10	0.04
67-3-27.5	**12.0**	**125**	**24.2**	**2.04**	**0.45**	**1.14**	**0.15**	**0.16**
2s		9.12	4.3	0.44	0.07	0.27	0.07	0.04
75-1-38.9	**12.5**	**94.4**	**23.2**	**1.99**	**0.42**	**1.03**	**0.21**	**0.17**
2s		22.3	4.2	0.43	0.07	0.24	0.09	0.04
79-3-150.4	**13.5**	**81.8**	**22.2**	**1.97**	**0.44**	**1.03**	**0.15**	**0.14**
2s		20.3	4.0	0.42	0.07	0.24	0.07	0.04
81-1-210.0	**24.5**	**60.7**	**12.7**	**1.65**	**0.21**	**0.57**	**0.06**	**0.09**
2s		4.51	2.3	0.36	0.04	0.14	0.03	0.02
67-3-6.8	**25.8**	**102**	**15.2**	**1.67**	**0.33**	**0.71**	**0.09**	**0.11**
2s		25.6	2.7	0.36	0.05	0.17	0.04	0.03
81-1-239.9	**26.6**	**52.9**	**12.4**	**1.66**	**0.21**	**0.56**	**0.05**	**0.08**
2s		3.86	2.2	0.36	0.04	0.13	0.02	0.02
81-1-169.9x	**26.9**	**91.9**	**16.0**	**1.78**	**0.39**	**0.95**	**0.11**	**0.11**
2s		6.85	2.9	0.38	0.06	0.22	0.05	0.03
81-1-119.2	**6.74**	**141**	**22.6**	**1.58**	**0.74**	**1.00**	**0.14**	**0.12**
2s		8.93	4.1	0.34	0.12	0.24	0.06	0.03
75-1-134.4	**10.9**	**126**	**19.0**	**1.52**	**0.74**	**1.42**	**0.09**	**0.13**
2s		7.99	3.4	0.33	0.12	0.34	0.04	0.03
79-3-160.3	**16.1**	**105**	**17.5**	**1.56**	**0.66**	**0.91**	**0.13**	**0.10**
2s		6.61	3.2	0.34	0.11	0.21	0.06	0.02
79-3-172.8	**18.71**	**95.3**	**14.0**	**1.38**	**0.61**	**0.85**	**0.46**	**0.10**
2s		6.02	2.51	0.30	0.10	0.20	0.20	0.02
81-1-294.7	**14.3**	**109**	**17.0**	**1.47**	**0.58**	**0.72**	**0.11**	**0.11**
2s		6.87	3.06	0.32	0.09	0.17	0.05	0.03

In	Sn	Sb	W	Tl	Pb	Bi
0.11	**2.75**	**0.09**	**0.68**	**0.03**	**1.18**	**0.03**
0.02	0.78	0.04	0.59	0.01	0.12	0.01
0.09	**4.66**	**0.09**	**0.36**	**0.02**	**7.48**	**0.03**
0.01	1.33	0.04	0.31	0.01	0.74	0.01
0.06	**1.30**	**0.15**	**0.32**	**0.02**	**1.73**	**0.03**
0.01	0.37	0.07	0.28	0.01	0.09	0.00
0.13	**7.11**	**0.30**	**1.04**	**0.08**	**4.82**	**0.08**
0.02	2.02	0.15	0.91	0.03	0.15	0.01
0.18	**7.27**	**0.30**	**1.28**	**0.10**	**5.42**	**0.07**
0.03	2.07	0.15	1.12	0.04	0.17	0.01
0.17	**5.44**	**0.28**	**0.93**	**0.08**	**6.54**	**0.07**
0.03	1.55	0.14	0.81	0.03	0.21	0.01
0.11	**3.57**	**0.14**	**0.52**	**0.04**	**2.45**	**0.02**
0.02	1.02	0.07	0.45	0.01	0.08	0.00
0.14	**3.34**	**0.13**	**0.41**	**0.04**	**1.38**	**0.05**

(*continued on next page*)

Table 2 (*continued*)

In	Sn	Sb	W	Tl	Pb	Bi
0.02	0.95	0.07	0.36	0.01	0.13	0.01
0.12	**2.30**	**0.09**	**0.35**	**0.03**	**1.18**	**0.02**
0.02	0.65	0.05	0.31	0.01	0.12	0.00
0.09	**1.67**	**0.13**	**0.22**	**0.03**	**1.08**	**0.01**
0.01	0.47	0.06	0.19	0.01	0.03	0.00
0.10	**1.80**	**0.08**	**0.49**	**0.01**	**1.99**	**0.01**
0.02	0.51	0.04	0.42	0.01	0.19	0.00
0.10	**1.65**	**0.06**	**0.52**	**0.02**	**0.74**	**0.01**
0.02	0.47	0.03	0.45	0.01	0.07	0.00
0.05	**0.77**	**0.03**	**0.07**	**0.01**	**0.64**	**0.01**
0.01	0.22	0.02	0.06	0.00	0.02	0.00
0.07	**1.34**	**0.05**	**0.18**	**0.01**	**0.83**	**0.02**
0.01	0.38	0.02	0.16	0.00	0.08	0.00
0.05	**0.69**	**0.03**	**0.06**	**0.01**	**0.42**	**0.01**
0.01	0.20	0.01	0.05	0.00	0.01	0.00
0.07	**1.25**	**0.05**	**0.17**	**0.02**	**0.81**	**0.03**
0.01	0.36	0.02	0.15	0.01	0.03	0.00
0.09	**1.99**	**0.07**	**0.26**	**0.02**	**1.41**	**0.01**
0.01	0.57	0.03	0.23	0.01	0.07	0.00
0.08	**1.62**	**0.05**	**0.51**	**0.02**	**1.55**	**0.01**
0.01	0.46	0.03	0.45	0.01	0.08	0.00
0.06	**1.24**	**0.05**	**0.21**	**0.01**	**1.01**	**0.02**
0.01	0.35	0.02	0.19	0.00	0.05	0.00
0.06	**1.06**	**0.04**	**0.16**	**0.01**	**1.02**	**0.01**
0.01	0.30	0.02	0.14	0.00	0.05	0.00
0.08	**1.32**	**0.05**	**0.19**	**0.02**	**0.89**	**0.02**
0.01	0.37	0.02	0.17	0.01	0.05	0.00

*2s denotes two standard deviations given repeated runs of USGS SRM BHVO-1 and AGV-2.

those found in other studies of basalts. Immiscible sulfide blebs that have been found in MORB (Peach et al., 1990; Patten et al., 2013), arc-related basalts (Jenner et al., 2015), and those experimentally synthesized in silicate melts (Li and Audétat, 2012, 2015; Kiseeva and Wood, 2015) are Fe- and Ni-rich and composed of mono-sulfide solution (MSS), pentlandite, and/or pyrrhotite compositions that were in equilibrium with more primitive magmas. By contrast, the Kilauea Iki groundmass sulfides are different in this respect because they are Cu-rich phases that are surrounded by an intermediate to felsic melt. Rare Ni-rich MSS sulfides are found as occasional inclusions in olivine and in the Iki-22 pumice groundmass, which likely originated deep in Kilauea's magma system. Sulfur analyses from scoria glasses suggest that the initial magma was not sulfide saturated (Helz et al., 2017).

Magnetite crystallization is proposed to cause sulfide saturation in basalts from the Lau and Manus back arc basins by redox reactions (Jenner et al., 2010, 2012; Jenner et al., 2015). In these magmas, sulfides form immediately following magnetite saturation at ~6 and 3 wt% MgO_{glass}, in the two basins, respectively. In KI, Fe-Ti oxides (titaniferous-magnetite, ilmenite, and pseudobrookite) crystallize and fractionate between 5 and 3 wt% MgO_{glass}, as evidenced by the decrease in Ti and Fe on whole rock and glass MgO variation diagrams (supplementary figures) and the appearance of these phases in thin section. This precedes sulfide saturation at 2 wt% MgO_{glass}. The incorporation of Fe^{3+} into magnetite and pseudobrookite will reduce the residual melt and drive sulfur reduction (S^{6+} to S^{2-}), leading to the formation of sulfides. Oxygen fugacities calculated using the Fe-Ti oxide oxy-thermobarometer of Ghiorso and Evans (2008) indicate that at the onset of magnetite crystallization, the fO_2 of the system was around NNO+1.5 (or roughly FMQ+2.3). No sulfides are observed in the groundmass of the more primitive samples as the oxygen fugacity is too high for sulfide to saturate (Jugo, 2009); this is also consistent with the sulfide undersaturation inferred for the primary magma (Helz et al., 2017). The oxygen fugacity falls to NNO−1 after the onset of the magnetite fractionation in the more evolved samples (supplementary figures). We propose that this process of magnetite-induced sulfide saturation, which has been termed the "magnetite crisis" (Jenner et al., 2010), contributes to sulfide saturation in KI.

In KI, the Cu-rich sulfides are present in even the most evolved samples, implying that they did not physically segregate from the differentiating magma. This suggests that the lava lake was effectively a closed system at this stage of its evolution such that the sulfide blebs were trapped within a semi-rigid crystal network (Fig. 1).

6.3. Behavior of nominally chalcophile elements

6.3.1. Chalcophile elements

We observed that Ag, Bi, Cd, and In are strongly chalcophile because their abundance in the melt is entirely controlled by sulfide saturation, i.e., they fractionate out of the

Table 3
Chalcophile element abundances (ppm) in glass. Major and other trace element data are presented in appendix Table A3.

	MgO wt%	Cu	Ga	Ge	As	Mo	Ag	Cd
67-3-75.0	**0.51**	**291**	**61.0**	**10.8**	**13.9**	**6.36**	**0.12**	**0.21**
2s	0.10	100	24.6	8.96	9.34	2.66	0.37	0.33
79-3-160.6	**0.61**	**133**	**44.9**	**4.45**	**7.72**	**7.75**	**0.12**	**0.22**
2s	0.06	18.8	11.3	1.95	2.37	2.48	0.00	0.32
79-3-171.9	**4.32**	**319**	**33.4**	**4.23**	**10.2**	**2.46**	**0.11**	**0.11**
2s	0.18	38.5	3.40	1.15	6.45	0.23	0.05	0.07
79-1R1-170.9	**1.78**	**333**	**35.1**	**5.63**	**6.68**	**3.06**	**0.11**	**0.21**
2s	0.22	68.7	1.83	0.61	1.72	0.64	0.03	0.15
81-1-209.8	**6.09**	**193**	**25.5**	**3.40**	**2.74**	**1.36**	**0.07**	**0.20**
2s	0.15	35.7	4.02	0.84	1.25	0.39	0.03	0.13
81-1-294.7	**5.03**	**314**	**33.9**	**4.36**	**4.22**	**2.15**	**0.14**	**0.11**
2s	0.39	24.5	3.79	0.76	1.39	0.37	0.02	0.24
81-1-169.9*	**0.14**	**18.6**	**32.8**	**3.11**	**15.8**	**8.29**	**0.06**	**0.17**
2s	0.06	1.23	7.16	1.62	ND	1.22	ND	0.34
79-3-158*	**0.37**	**67.3**	**38.3**	**4.95**	**6.77**	**4.43**	**0.09**	**0.15**
2s	0.12	11.1	6.27	1.70	2.06	1.27	0.01	0.19
67-3-75.7	**0.58**	**162**	**44.7**	**6.76**	**ND**	**4.73**	**0.09**	**ND**
2s	0.13	21.5	3.94	1.33	ND	0.44	0.02	ND
67-3-75.7b*	**0.49**	**122**	**36.7**	**5.65**	**9.18**	**4.18**	**0.12**	**0.21**
2s	0.13	12.6	3.51	0.74	2.29	1.51	0.04	0.16
75-1-134.4	**2.01**	**225**	**54.6**	**8.69**	**11.9**	**5.17**	**0.11**	**0.23**
2s	0.07	36.2	8.41	3.21	4.68	0.56	0.06	0.17
81-1-178.6b	**0.79**	**189**	**69.8**	**7.73**	**6.39**	**8.23**	**0.25**	**0.12**
2s	0.18	26.9	24.0	6.20	1.13	1.18	ND	0.03
81-1-178.6sv	**0.52**	**119**	**17.9**	**6.53**	**ND**	**3.78**	**0.15**	**ND**
2s	0.04	53.9	30.9	2.86	2.86	1.08	0.03	ND
67-3-70.0	**0.09**	**116**	**44.1**	**5.79**	**8.64**	**5.10**	**0.18**	**0.16**
2s	0.05	100	12.1	4.29	5.60	3.31	ND	0.14
67-3-83.7	**1.77**	**344**	**63.1**	**10.4**	**ND**	**7.53**	**0.15**	**ND**
2s	0.81	119	17.9	6.53	ND	3.78	ND	ND
67-3-76.2*	**0.66**	**193**	**60.0**	**9.00**	**12.5**	**6.26**	**0.06**	**0.24**
2s	0.20	79.0	23.9	3.90	8.97	3.13	0.06	0.31
75-1-130.5	**0.40**	**75.4**	**44.5**	**4.95**	**14.8**	**8.55**	**0.10**	**0.24**
2s	0.07	10.7	22.1	5.02	ND	2.39	0.03	0.23
75-1-125.0*	**0.09**	**29.1**	**34.9**	**3.29**	**6.08**	**3.77**	**0.13**	**0.10**
2s	0.04	4.21	3.64	1.77	1.96	1.90	0.01	0.08
79-3-160.6i	**3.24**	**32.8**	**23.3**	**2.69**	**6.10**	**0.88**	**0.08**	**0.05**
2s	0.31	7.07	0.57	0.25	ND	0.18	0.13	ND
79-3-171.9i	**5.06**	**148**	**23.1**	**2.80**	**4.96**	**0.88**	**0.08**	**0.24**
2s	0.25	32.4	3.38	0.69	3.92	0.25	0.11	0.23
81-1-209.8i	**6.06**	**191**	**25.2**	**2.40**	**3.20**	**1.45**	**0.07**	**0.33**
2s	0.08	*1 analysis*						

In	Sn	Sb	W	Tl	Pb	Bi
0.07	**9.45**	**0.29**	**1.82**	**0.22**	**10.1**	**0.07**
0.02	2.17	0.33	0.70	0.09	1.53	0.04
0.23	**7.36**	**0.36**	**2.12**	**0.22**	**7.62**	**0.06**
0.49	2.35	0.35	0.81	0.09	1.54	0.02
0.13	**2.54**	**0.12**	**0.60**	**0.04**	**ND**	**0.03**
0.05	0.66	0.08	0.21	0.04	ND	0.01
0.15	**3.85**	**0.15**	**0.82**	**0.07**	**6.15**	**0.04**
0.02	0.66	0.17	0.20	0.04	0.98	0.03
0.10	**1.68**	**0.04**	**0.34**	**0.03**	**1.70**	**0.01**
0.06	0.84	0.06	0.14	0.03	0.54	0.03
0.13	**3.11**	**0.05**	**0.53**	**0.06**	**2.72**	**0.04**
0.05	0.89	0.13	0.11	0.04	0.06	0.03
0.06	**6.44**	**0.90**	**2.39**	**0.32**	**ND**	**0.03**
0.02	2.09	0.44	0.65	0.13	ND	0.02
0.10	**7.07**	**0.24**	**1.58**	**0.15**	**7.74**	**0.04**
0.03	1.54	0.14	0.37	0.04	1.04	0.02

(*continued on next page*)

Table 2 (*continued*)

In	Sn	Sb	W	Tl	Pb	Bi
0.22	**7.22**	**0.30**	**1.47**	**0.15**	ND	**0.04**
0.18	1.56	0.12	0.29	0.05	ND	0.03
0.09	**7.30**	**0.45**	**1.40**	**0.10**	**7.38**	**0.05**
0.06	1.99	0.82	0.80	0.10	ND	0.03
0.14	**6.05**	**0.23**	**1.26**	**0.13**	**6.37**	**0.05**
0.03	1.05	0.09	0.27	0.04	0.86	0.03
0.08	**8.80**	**0.45**	**2.16**	**0.26**	**ND**	**0.04**
0.06	5.21	0.23	0.72	0.03	ND	0.04
0.11	**3.63**	**1.71**	**0.92**	**0.15**	**ND**	**0.06**
0.04	1.42	0.17	0.23	0.03	ND	ND
0.06	**8.32**	**0.33**	**1.75**	**0.15**	**ND**	**0.03**
0.06	4.12	0.26	1.21	0.13	ND	0.04
0.15	**8.48**	**0.92**	**2.18**	**0.16**	**ND**	**0.09**
0.06	3.63	1.71	0.92	0.15	ND	0.06
0.10	**7.97**	**0.28**	**1.91**	**0.17**	**8.00**	**0.05**
0.04	2.11	0.17	1.13	0.11	2.53	0.05
0.06	**8.42**	**0.42**	**2.51**	**0.21**	**ND**	**0.06**
0.02	2.57	0.31	0.89	0.08	ND	0.05
0.09	**10.1**	**0.37**	**2.15**	**0.20**	**ND**	**0.04**
0.02	1.81	0.21	0.44	0.08	ND	0.02
0.26	**1.11**	**0.15**	**0.21**	**0.01**	**ND**	**0.01**
0.03	0.45	0.08	0.12	0.00	ND	0.00
0.21	**1.26**	**0.07**	**0.21**	**0.02**	**ND**	**0.03**
0.21	0.58	0.13	0.20	0.04	ND	0.02
0.23	**2.87**	**0.07**	**0.30**	**0.02**	**ND**	**0.04**

*Starred and underlined samples contain sulfides analyzed with laser ablation. Glass concentrations are used in D value calculations (Table 5).

*2s denotes two standard errors of the mean of multiple point analyses.

evolving melt when sulfides form. By contrast, Pb and Sn concentrations continue to increase in the evolving melt (Fig. 4), so their behavior in the magma is not entirely controlled by sulfide saturation. This is due to the lower $D^{\text{sulfide/silicate melt}}$ of Pb and Sn and exceedingly small volume of sulfides that precipitate in this system. The sulfides are abundant enough to deplete the concentrations of the strongly chalcophile elements from the silicate melt, but not Pb and Sn. Lead analyses were added to the study late, thus not all glass samples plotted in Fig. 4 have corresponding Pb data. This may potentially skew interpretations because the absolute lowest MgO samples were not analyzed for Pb – missing data could reveal that Pb does drop in abundance in the most evolved samples. The average Nd/Pb ratio of the whole rock samples is 19 (±9 2SD) which is consistent with an average of 15 for OIB (Hofmann, 2003; Hart and Gaetani, 2006). This ratio does not change systematically with differentiation in either the whole rock or glass data, suggesting that Pb and Nd (and Ce) do behave similarly, consistent with Pb not being strongly influenced by sulfide saturation.

In sulfides found in MORB (Patten et al., 2013), Ag, Bi, Cd, Pb, and Sn were also found to be chalcophile and calculated D values agree with those determined here (Fig. 5, enclosed circles, In was not measured in the Patten et al. study). This is an interesting observation given the differing melt composition, sulfide composition, and intensive variables (T, P, and fO_2) between the Kilauea Iki lava and MORB. MORBs saturate Ni-rich sulfides at around 10 wt % MgO_{glass} which is not induced by magnetite saturation (Jenner and O'Neill, 2012; Patten et al., 2013). Hart and Gaetani (2016) experimentally determined Pb $D^{\text{sulfide liquid/silicate melt}}$ values to be between 4 and 66, dependent on T and FeO_{glass}, with expected MORB $D \sim 45$. Additionally, Li and Audétat (2012) produced experimental $D^{\text{sulfide liquid/silicate melt}}$ that match those calculated for Ag, Bi, Pb, and Sn in KI (Fig. 5, X's, no Cd or In data are available in the Li and Audétat study; data were selected from runs having the composition, fO_2, and P and T conditions near those of KI; the sulfide composition has between 1.8 and 3.0 wt% Cu). Finally, the experimental work of Kiseeva and Wood (2013, 2015) produced an algorithm that incorporates temperature, sulfide composition, and melt composition to calculate $D^{\text{sulfide/silicate melt}}$; D values calculated from this equation at the range in T, $Cu_{sulfide}$, and FeO_{glass} found in KI generally reproduce the KI partition coefficients quite well (gray bars, Fig. 5). In KI, there is no correlation between $D^{\text{sulfide/silicate melt}}$ and MgO_{glass} or FeO_{glass} (which is directly related to the oxygen content of the sulfide, Kiseeva and Wood, 2015). However, the samples that contain sulfides cover a small range of MgO_{glass} or FeO_{glass} so trends may not be observable given the limited range of melt compositions. Additionally, there is no correlation between sulfide compositions (Cu, Fe, S, Ni, Mn, or Co content) and $D^{\text{sulfide/silicate melt}}$.

6.3.2. Weakly chalcophile and non-chalcophile elements

Arsenic, Ge, Sn, Tl, Mo, Ga, and W are weakly chalcophile to non-chalcophile (i.e., lithophile) in this igneous system (Fig. 5). Of these elements, Mo was also measured in MORB sulfides and found to be weakly chalcophile (Patten et al., 2013). KI D values for As, Sb, Mo, and W

Table 4
Chalcophile element abundances (ppm) in sulfides.

Sulfide	Spot size, μm	Ga	Ge	As	Mo	Ag	Cd
Sample 67-3-75.7b							
75.7b_S02b	**30**	**0.18**	**6.50**	**200**	**2.56**	**70.1**	**30.7**
2s		0.52	1.48	47.0	0.70	6.86	4.88
75.7b_S03	**30**	**0.26**	**8.85**	**104**	**1.46**	**40.6**	**24.6**
2s		0.34	1.38	20.2	0.44	4.49	3.25
75.7b_S04	**55**	**0.34**	**6.63**	**83.0**	**1.92**	**104**	**32.0**
2s		0.09	0.58	14.5	0.27	9.55	1.70
75.7b_S08	**40**	**4.51**	**5.45**	**95.0**	**1.40**	**93.0**	**20.5**
2s		0.69	0.71	19.1	0.39	8.49	1.63
75.7b_S11b	**55**	**3.98**	**5.21**	**22.4**	**2.25**	**83.8**	**30.4**
2s		0.66	0.61	5.94	0.33	5.94	2.12
75.7b_S12a	**65**	**0.40**	**8.56**	**89.0**	**1.69**	**169**	**61.5**
2s		0.07	0.61	13.8	0.24	6.93	2.83
75.7b_S13b	**40**	**2.59**	**9.40**	**71.0**	**1.54**	**108**	**6.40**
2s		0.54	1.20	14.1	0.36	7.78	1.27
75.7b_S14	**55**	**0.47**	**8.70**	**8.70**	**1.16**	**85.3**	**49.7**
2s		0.14	0.81	0.92	0.24	3.64	3.08
Sample 75-1-125.0							
125.0_S02	**25**	**1.70**	**14.9**	**10.3**	**7.40**	**110**	**76.0**
2s		0.92	2.76	2.55	2.19	21.9	11.3
125.0_S05	**30**		**6.35**	**4.85**	**0.49**	**47.0**	**65.0**
2s			1.13	1.13	0.31	3.54	8.49
125.0_S08	**30**	**1.04**	**7.40**	**11.6**	**4.55**	**95.0**	**71.0**
2s		0.47	1.56	2.37	1.41	12.7	11.0
125.0_S12	**25**	**0.25**	**6.75**	**6.90**	**1.36**	**115**	**52.0**
2s		0.30	1.67	1.95	0.61	15.6	8.14
125.0_S13	**30**	**0.35**	**5.60**	**3.01**	**0.53**	**30.7**	**44.3**
2s		0.23	0.95	0.78	0.23	2.57	5.39
125.0_S15a	**30**	**1.12**	**8.00**	**12.8**	**5.05**	**86.5**	**92.0**
2s		0.64	1.80	2.05	1.34	5.41	10.6
125.0-S17	**30**	**1.35**	**7.00**	**2.70**	**0.39**	**44.9**	**47.5**
2s		0.56	1.48	0.85	0.22	4.95	7.43
125.0_S27	**25**	**1.95**	**8.95**	**10.6**	**bdl**	**33.1**	**38.4**
2s		1.23	3.13	2.84		6.13	9.53
125.0_S34	**25**	**2.90**	**10.2**	**16.0**	**3.85**	**114**	**80.0**
2s		1.70	3.51	3.79	1.06	9.92	15.9
Sample 67-3-76.2							
76.2_S04	**40**	**9.80**	**8.10**	**8.40**	**1.36**	**94.0**	**34.8**
2s		2.44	1.38	2.19	0.45	9.55	5.06
76.2_S05	**55**	**0.29**	**10.1**	**9.50**	**0.79**	**89.0**	**42.1**
2s		0.11	0.88	1.42	0.22	7.43	3.29
76.2_S06	**40**	**0.18**	**5.61**	**4.05**	**0.63**	**81.1**	**26.8**
2s		0.08	0.80	0.58	0.20	6.82	2.62
76.2_S13	**40**	**0.62**	**6.15**	**3.38**	**0.65**	**168**	**22.8**
2s		0.21	0.83	0.55	0.21	19.2	2.42
76.2_S01	**55**	**0.27**	**5.13**	**6.21**	**1.14**	**96.2**	**34.5**
2s		0.08	0.50	0.55	0.14	5.23	2.19
Sample 81-1-169.9							
169.9_S05	**40**	**22.3**	**5.70**	**9.20**	**8.35**	**76.4**	**49.3**
2s		6.12	1.49	2.27	1.67	5.31	5.31
169.9_S09	**30**	**1.15**	**7.05**	**2.35**	**0.90**	**70.5**	**33.4**
2s		1.30	2.48	0.90	0.67	13.0	8.99
Sample 79-3-158.0							
158_S28	**30**	**0.52**	**4.50**	**6.00**	**1.91**	**112**	**73.0**
2s		0.69	3.70	2.40	0.82	18.0	14.00
158_S30	**25**		**12.5**	**7.60**	**3.30**	**291**	**217**
2s		0.83	9.30	5.50	2.40	40.0	57.0
158_S23	**25**	**0.20**	**4.70**	**3.20**	**7.20**	**158**	**95.0**
2s		0.75	5.30	3.30	3.70	31.0	26.0

(*continued on next page*)

Table 4 (*continued*)

Sulfide	Spot size, μm	Ga	Ge	As	Mo	Ag	Cd
158_S20	**30**	**0.14**	**5.60**	**1.60**	**2.81**	**80.0**	**59.0**
2s		0.25	2.30	1.80	0.85	12.0	10.0
158_S22	**30**	**0.19**	**8.80**	**4.20**	**4.00**	**124**	**108**
2s		0.60	4.50	2.70	1.90	21.0	21.0
158_S11	**40**	**5.00**	**10.9**	**9.40**	**7.80**	**355**	**127**
2s		1.20	2.50	2.40	1.50	65.0	11.0
158_S12	**30**		**4.90**	**3.30**	**3.11**	**148**	**80.0**
2s		0.21	2.50	1.80	0.90	26.0	16.0

In	Sn	Sb	W	Tl	Pb	Bi
2.78	**27.7**	**0.23**	**0.10**	**0.03**	**320**	**32.2**
0.40	5.27	0.47	0.12	0.04	19.4	3.36
1.46	**25.0**	**0.18**	**bdl**	**bdl**	**257**	**21.0**
0.30	4.28	0.18	0.71	0.01	16.6	1.59
2.87	**22.1**	**0.39**	**0.02**	**0.20**	**342**	**21.5**
0.24	1.77	0.08	0.02	0.04	13.1	0.88
3.22	**24.6**	**0.51**	**0.09**	**0.09**	**334**	**8.89**
0.27	2.72	0.11	0.05	0.06	13.1	0.70
2.68	**25.8**	**0.46**	**0.21**	**0.19**	**318**	**27.8**
0.20	1.87	0.08	0.06	0.04	12.4	1.31
3.05	**39.7**	**0.64**	**0.02**	**0.32**	**311**	**30.1**
0.17	2.44	0.10	0.01	0.05	11.0	1.27
2.17	**20.0**	**0.81**	**0.12**	**0.20**	**247**	**10.5**
0.25	2.83	0.23	0.08	0.07	13.4	0.71
2.39	**32.7**	**0.54**	**0.02**	**0.17**	**274**	**25.6**
0.19	2.51	0.13	0.02	0.05	12.0	1.20
3.93	**78.0**	**1.06**	**bdl**	**0.53**	**909**	**33.2**
0.78	12.7	0.48	0.71	0.30	57.3	3.54
3.53	**5.35**	**0.33**	**bdl**	**0.05**	**314**	**35.3**
0.31	1.52	0.18	0.71	0.05	13.8	2.37
4.67	**76.5**	**0.77**	**bdl**	**bdl**	**970**	**38.4**
0.50	12.0	0.48	0.71	0.71	84.9	5.06
3.96	**55.0**	**0.30**	**0.22**	**bdl**	**636**	**20.9**
0.53	8.85	0.20	0.22	0.71	40.4	1.74
2.53	**2.11**	**0.10**	**bdl**	**bdl**	**27.6**	**3.54**
0.22	0.95	0.08	0.71	0.71	1.86	0.38
7.33	**101**	**0.46**	**0.15**	**0.02**	**911**	**26.3**
0.78	11.7	0.27	0.21	0.03	51.3	3.85
3.83	**2.25**	**0.06**	**0.02**	**bdl**	**19.1**	**1.89**
0.46	0.92	0.06	0.03	0.71	1.87	0.31
4.46	**4.00**	**bdl**	**bdl**	**bdl**	**25.8**	**6.30**
0.73	2.39				2.80	1.23
8.32	**88.0**	**0.61**	**bdl**	**0.46**	**818**	**26.3**
0.85	16.7	0.48	0.71	0.31	57.8	3.08
3.21	**27.3**	**0.44**	**0.30**	**0.23**	**227**	**26.5**
0.30	5.06	0.19	0.19	0.13	18.7	3.61
3.27	**36.0**	**0.36**	**bdl**	**0.19**	**245**	**26.2**
0.21	8.14	0.10	0.71	0.04	11.3	3.22
1.26	**13.0**	**0.18**	**bdl**	**bdl**	**125**	**10.8**
0.14	2.28	0.09	0.71	0.71	5.26	0.81
1.95	**28.9**	**0.39**	**0.03**	**bdl**	**156**	**15.8**
0.19	4.63	0.15	0.03	0.71	6.58	1.99
1.29	**43.5**	**0.43**	**0.01**	**0.14**	**375**	**18.6**
0.13	2.62	0.10	0.01	0.04	12.0	0.99
4.35	**73.9**	**0.72**	**0.93**	**1.75**	**994**	**23.2**
0.35	6.48	0.23	0.34	0.38	38.9	1.95
3.68	**25.0**	**0.12**	**0.06**	**bdl**	**350**	**17.3**
0.33	6.19	0.17	0.08	0.71	23.0	1.86
2.97	**31.9**	**0.45**	**bdl**	**0.16**	**nd**	**37.9**

(*continued on next page*)

Table 4 (*continued*)

In	Sn	Sb	W	Tl	Pb	Bi
0.94	5.80	0.42		0.12		6.30
6.51	**78.0**	**bdl**	**bdl**	**bdl**	**nd**	**29.4**
2.80	18.0					5.70
2.19	**34.2**	**0.15**	**bdl**	**bdl**	**nd**	**59**
1.20	9.30	0.39				20.0
2.20	**33.4**	**0.30**	**bdl**	**0.03**	**nd**	**23.5**
0.79	5.30	0.33		0.05		3.80
3.38	**58.0**	**1.80**	**bdl**	**bdl**	**nd**	**35.9**
1.00	17.0	1.10				9.90
4.32	**69.2**	**0.67**	**0.24**	**0.13**	**nd**	**58.1**
0.76	7.60	0.33	0.15	0.07		5.50
4.53	**29.1**	**0.22**	**bdl**	**bdl**	**nd**	**26.9**
0.62	8.70	0.25				9.50

agree with those determined in the Li and Audétat (2012) study. Germanium, Tl, and Ga partition coefficients are in agreement (within error) with those predicted by the Kiseeva & Wood calculation, however the KI D_{Sb} falls significantly below the predicted values.

The abundance of Ga, Ge, and As appear to drop in the glasses at around 2 wt% MgO_{glass} (Fig. 4). This drop may be partially attributed to partitioning into sulfides for As and Ge, but Ga would not be affected by sulfide saturation. Instead, we propose that these elements, specifically As, may partition into apatite, where they substitute for P. While apatite is a common accessory phase in the evolved samples, it forms thin (<5 μm wide) needles that are too small for laser ablation analyses to confirm the presence of these elements. Additionally, minor Ga substitutes for Al and Ge may substitute for Si in late fractionating plagioclase or augite. Scatter in the Mo and Ga abundances in evolved samples (Fig. 4) is likely caused by partitioning into Fe-Ti oxides. Antimony, Tl, Mo, and W are not significantly affected by sulfide saturation and instead behave as overall incompatible, lithophile elements during differentiation from mafic to felsic magmas. Octahedrally coordinated Mo and W have ionic radii that differ by only 1%, so their substitution for Ti in Ti-oxides is expected to be roughly equal, however Mo is significantly more abundant in oxides than W. The reason for this difference in partitioning into oxides is unknown, however it may simply be attributed to Mo being more abundant in the system than W (Mo/W ratios vary between 2 and 4 in the glass). Additionally, Mo is slightly more chalcophile than W. Despite this, Mo and W generally behave as incompatible lithophile elements in this system.

6.4. Molybdenum in basalts

Molybdenum is an element of special interest because of its redox-sensitivity, suggested chalcophile behavior, and use as a paleo-redox indicator for Precambrian surface and ocean environments. Molybdenum is a chalcophile element in hydrothermal/epithermal systems that carry sufficient quantities of reduced S (MoS_2 formation) and in anoxic marine environments where it is sequestered in authigenic Fe-Mo-S phases (Helz et al., 2011) or converted to tetrathiomolybdate particles (MoS_4^{2-}) that settle out of solution (Erickson and Helz, 2000). However, in the KI magmatic system it shows incompatible, lithophile behavior and is more heavily concentrated in glass (average 5 ppm) and Fe-Ti oxides (average 6.4 ppm) than sulfides (average 2.6 ppm). Considering the abundances of these different phases, the glass accounts for the majority of the Mo in the samples (between ~50 and ~90%). The Mo $D^{sulfide/silicate}$ values measured here corroborate those from a study of MORB that found Mo concentrations in sulfides were often below the detection limit of LA-ICP-MS (Patten et al., 2013). Molybdenum occurs primarily in its oxidized, hexavalent state in the basaltic glass (O'Neill and Eggins, 2002), making it generally incompatible in most silicates and incapable of bonding with S^{2-} to form MoS_2. Hexavalent Mo likely substitutes for octahedrally coordinated tetravalent Ti^{4+} in ilmenite as well as tetrahedrally coordinated Ti^{4+} in pseudobrookite, given similar ionic radii. Hexavalent Mo substitution into Fe-Ti-oxides would need to be charge balanced to maintain electrical neutrality.

A crustal sulfide host of Mo has been invoked in paleoatmosphere studies (Anbar et al., 2007) where oxidative weathering of pyrite and molybdenite is suggested to release Mo from the continental crust at the time of the Great Oxidation Event (GOE). Here we show that sulfide blebs comprising three common igneous sulfides – chalcopyrite, isocubanite, and bornite – do not host significant Mo. In fact, mass balance calculations suggest that the sulfides typically host less than 5% of the total Mo budget of the samples in Kilauea Iki. We conclude that sulfides are not a significant host of Mo in basalts (MORB) and andesites (evolved KI), while glass and, to a lesser extent, magnetite and ilmenite are. Thus, the oxidation of igneous sulfides is likely not an important source of Mo to the oceans. This has significance for the use of Mo as a paleo-redox proxy as the Archean upper continental crust was significantly more mafic (Taylor and McLennan, 1985; Tang et al., 2016: Gaschnig et al., 2016) and the felsic continents were likely smaller (Cawood et al., 2013) and basalt was probably a much more common crustal lithology. The weathering properties of Mo-rich basaltic to komatiitic glass should be investigated in order to understand Mo removal from the crust at the time of the GOE.

6.5. Enrichments of As, Ag, Sb, W, and Bi

In KI whole rock powders and glasses, several chalcophile and lithophile elements are systematically enriched

Table 5
Partition coefficients (D) between sulfide and glass.

Sulfide	Ga	Ge	As	Mo	Ag	Cd
Sample 67-3-75.7b						
75.7b_S02b	**0.00**	**1.15**	**21.8**	**0.61**	**567**	**148**
2s	0.01	0.30	7.47	0.28	520	826
75.7b_S03	**0.01**	**1.57**	**11.3**	**0.35**	**328**	**118**
2s	0.01	0.32	3.58	0.16	302	661
75.7b_S04	**0.01**	**1.17**	**9.04**	**0.46**	**837**	**154**
2s	0.00	0.18	2.75	0.18	768	861
75.7b_S08	**0.12**	**0.96**	**10.3**	**0.33**	**752**	**99**
2s	0.02	0.18	3.32	0.15	690	551
75.7b_S11b	**0.11**	**0.92**	**2.43**	**0.54**	**678**	**147**
2s	0.02	0.16	0.89	0.21	620	819
75.7b_S12a	**0.01**	**1.51**	**9.69**	**0.40**	**1369**	**296**
2s	0.00	0.23	2.85	0.16	1250	1655
75.7b_S13b	**0.07**	**1.66**	**7.73**	**0.37**	**874**	**31**
2s	0.02	0.30	2.47	0.16	800	172
75.7b_S14	**0.01**	**1.54**	**0.95**	**0.28**	**690**	**239**
2s	0.00	0.25	0.26	0.12	630	1337
Sample 75-1-125.0						
125.0_S02	**0.05**	**4.54**	**1.69**	**1.96**	**848**	**779**
2s	0.03	2.58	0.69	1.15	1060	682
125.0_S05	**0.00**	**1.93**	**0.80**	**0.13**	**362**	**666**
2s		1.09	0.32	0.10	447	581
125.0_S08	**0.03**	**2.25**	**1.91**	**1.21**	**733**	**727**
2s	0.01	1.30	0.73	0.71	909	638
125.0_S12	**0.01**	**2.05**	**1.14**	**0.36**	**883**	**533**
2s	0.01	1.22	0.49	0.24	1096	467
125.0_S13	**0.01**	**1.70**	**0.49**	**0.14**	**236**	**454**
2s	0.01	0.96	0.21	0.09	*292*	395
125.0_S15a	**0.03**	**2.44**	**2.10**	**1.34**	**667**	**943**
2s	0.02	1.42	0.76	0.76	824	821
125.0-S17	**0.04**	**2.13**	**0.44**	**0.10**	**346**	**487**
2s	0.02	1.23	0.20	0.08	428	427
125.0_S27	**0.06**	**2.72**	**1.74**	**0.00**	**255**	**393**
2s	0.04	1.75	0.73		*318*	353
125.0_S34	**0.08**	**3.09**	**2.62**	**1.02**	**875**	**820**
2s	0.05	1.97	1.05	0.59	1082	726
Sample 67-3-76.2						
76.2_S04	**0.16**	**0.90**	**0.67**	**0.22**	**1522**	**142.8**
2s	0.08	0.42	0.51	0.13	1493	182
76.2_S05	**0.00**	**1.12**	**0.76**	**0.13**	**1441**	**173**
2s	0.00	0.49	0.56	0.07	1411	219
76.2_S06	**0.00**	**0.62**	**0.32**	**0.10**	**1313**	**110**
2s	0.00	0.28	0.24	0.06	1286	139
76.2_S13	**0.01**	**0.68**	**0.27**	**0.10**	**2721**	**93.5**
2s	0.01	0.31	0.20	0.06	2672	119
76.2_S01	**0.00**	**0.57**	**0.50**	**0.18**	**1558**	**142**
2s	0.00	0.25	0.36	0.09	1522	179
Sample 81-1-169.9						
169.9_S05	**0.68**	**1.83**	**0.58**	**1.01**	**1273**	**290**
2s	0.24	1.07	0.44	0.25	1249	579
169.9_S09	**0.04**	**2.27**	**0.15**	**0.11**	**1175**	**196**
2s	0.04	1.43	0.11	0.08	1152	395
Sample 79-3-158.0						
158_S28	**0.01**	**0.91**	**0.89**	**0.43**	**1227**	**488**
2s	0.02	0.81	0.45	0.22	1025	632
158_S30	**nd**	**2.52**	**1.12**	**0.74**	**3189**	**1451**
2s		2.07	0.88	0.58	2663	1896
158_S23	**0.01**	**0.95**	**0.47**	**1.62**	**1732**	**635**
2s	0.02	1.12	0.51	0.96	1446	831

(*continued on next page*)

Table 5 (*continued*)

Sulfide	Ga	Ge	As	Mo	Ag	Cd
158_S20	**0.00**	**1.13**	**0.24**	**0.63**	**877**	**395**
2s	0.01	0.61	0.28	0.26	732	509
158_S22	**0.00**	**1.78**	**0.62**	**0.90**	**1359**	**722**
2s	0.02	1.09	0.44	0.50	1135	935
158_S11	**0.13**	**2.20**	**1.39**	**1.76**	**3890**	**849**
2s	0.04	0.91	0.55	0.61	3249	1089
158_S12	**0.00**	**0.99**	**0.49**	**0.70**	**1622**	**535**
2s		0.61	0.30	0.29	1354	693

In	Sn	Sb	W	Tl	Pb	Bi
30.9	**3.79**	**0.51**	**0.07**	**0.31**	**43.3**	**662**
11.9	1.26	1.41	0.10	0.46	6.60	354
16.2	**3.42**	**0.39**	**nd**	**nd**	**34.8**	**431**
6.3	1.10	0.82			5.36	229
31.8	**3.02**	**0.86**	**0.01**	**1.94**	**46.3**	**442**
12.3	0.86	1.57	0.01	1.92	6.70	233
35.8	**3.36**	**1.12**	**0.06**	**0.85**	**45.3**	**183**
13.8	0.99	2.06	0.05	1.00	6.57	97
29.8	**3.53**	**1.01**	**0.15**	**1.86**	**43.0**	**572**
11.5	1.00	1.85	0.10	1.84	6.24	302
33.9	**5.43**	**1.41**	**0.02**	**3.14**	**42.1**	**618**
13.1	1.52	2.58	0.01	3.08	6.07	326
24.1	**2.74**	**1.80**	**0.09**	**2.00**	**33.5**	**216**
9.3	0.84	3.32	0.07	2.04	5.02	114
26.5	**4.47**	**1.19**	**0.01**	**1.65**	**37.1**	**526**
10.2	1.27	2.19	0.01	1.66	5.44	277
42.7	**7.76**	**2.88**	**nd**	**2.64**	**nd**	**893**
9.3	1.88	2.09		1.85		521
38.4	**0.53**	**0.88**	**nd**	**0.24**	**nd**	**948**
8.4	0.18	0.71		0.25		547
50.8	**7.61**	**2.09**	**nd**	**nd**	**nd**	**1033**
11.0	1.82	1.76				607
43.1	**5.47**	**0.80**	**0.10**	**nd**	**nd**	**562**
9.4	1.32	0.71	0.11			326
27.6	**0.21**	**0.27**	**nd**	**nd**	**nd**	**95.2**
6.0	0.10	0.27				55.5
79.7	**10.0**	**1.24**	**0.07**	**0.11**	**nd**	**708**
17.3	2.15	1.02	0.10	0.17		418
41.7	**0.22**	**0.15**	**0.01**	**nd**	**nd**	**50.9**
9.1	0.10	0.17	0.01			30.3
48.6	**0.40**	**nd**	**nd**	**nd**	**nd**	**170**
10.6	0.25					103
90.6	**8.76**	**1.66**	**nd**	**2.29**	**nd**	**706**
19.7	2.28	1.60		1.81		413
31.6	**3.42**	**1.58**	**0.15**	**1.30**	**28.3**	**526**
104	1.10	1.18	0.13	1.08	9.24	511
32.2	**4.52**	**1.30**	**0.00**	**1.08**	**30.6**	**520**
106	1.57	0.89		0.71	9.77	504
12.4	**1.62**	**0.65**	**0.00**	**0.00**	**15.7**	**215**
40.8	0.52	0.51			5.0	208
19.2	**3.62**	**1.41**	**0.01**	**0.00**	**19.5**	**313**
63.0	1.12	1.03	0.02		6.2	304
12.7	**5.46**	**1.56**	**0.00**	**0.82**	**46.9**	**370**
41.7	1.48	1.02	0.00	0.55	14.9	356
69.0	**11.5**	**0.80**	**0.39**	**5.46**	**nd**	**911**
20.3	3.86	0.47	0.18	2.51		581
58.5	**3.87**	**0.13**	**0.02**	**nd**	**nd**	**681**
17.2	1.58	0.20	0.04			436
29.5	**4.51**	**1.86**	**nd**	**1.10**	**nd**	**1585**
8.48	1.28	2.05		0.88		1446

(*continued on next page*)

Table 5 (*continued*)

In	Sn	Sb	W	Tl	Pb	Bi
64.5	**11.03**	**0.00**	**nd**	**nd**	**nd**	**1230**
18.6	3.50					1128
21.7	**4.84**	**0.62**	**nd**	**nd**	**nd**	**2468**
6.25	1.68	1.65				2365
21.8	**4.72**	**1.24**	**nd**	**0.23**	**nd**	**983**
6.28	1.27	1.54		0.32		895
33.5	**8.20**	**7.42**	**nd**	**nd**	**nd**	**1502**
9.65	2.99	6.30				1409
42.8	**9.79**	**2.76**	**nd**	**0.87**	**nd**	**2430**
12.3	2.38	2.12	0.10	0.53		2191
44.8	**4.11**	**0.91**	**nd**	**nd**	**nd**	**1125**
12.9	1.52	1.16				1084

Table 6
Average partition coefficients ($D^{oxide/glass}$) calculated for Fe-Ti oxides ilmenite and pseudobrookite. Complete trace element and partition coefficient data is listed in the appendix Table A4.

	Cu	Ga	Ge	As	Mo	Ag	Cd
pseudobrookite	**1.08**	**1.12**	**0.24**	**0.14**	**1.40**	**3.06**	**1.05**
2s	1.79	1.08	0.23	0.26	3.37	5.89	1.23
ilmenite	**0.47**	**0.38**	**0.24**	**0.25**	**0.53**	**3.59**	**0.97**
2s	0.51	0.32	0.82	0.92	0.57	7.12	1.96

In	Sn	Sb	W	Tl	Pb	Bi
2.44	**0.61**	**0.18**	**0.13**	**0.20**	**0.03**	**0.33**
4.69	0.91	0.29	0.21	0.73	0.09	0.33
2.95	**0.63**	**0.27**	**0.12**	**0.11**	**0.00**	**0.39**
4.48	0.76	1.15	0.21	0.23	0.01	0.50

relative to elements of similar compatibility, as determined by their anomalous peaks on a primitive mantle-normalized spider diagram (supplementary figures) and cross plots (Fig. 6). Enriched lavas plot in the upper right quadrant of Fig. 6, while MORB data (Jenner and O'Neill, 2012) plot around or slightly below one. Also shown in the cross plots are primitive glasses from the Eastern Manus back arc basin and Northwest Lau spreading center from Jenner et al. (2012). Interestingly, the subduction-influenced Manus BAB shares As, Sb, and Bi enrichments with Kilauea, while the NW Lau spreading center basalts lack signatures of subduction-influenced magmatism, and are not enriched in As or Bi. Thus, the As, Sb, and Bi budget of KI shares similarities with basalts influenced by recycling in subduction zones, however the W enrichment observed in KI lavas is not found in either back arc basin. The enrichment in Bi is especially striking considering its abundance may have been affected by degassing (Norman et al., 2004; and Section 6.1). In arc settings, enrichments in As, Sb, Tl, Pb, and Bi have been attributed to the influence of hydrothermally altered oceanic crust that concentrates these elements into low-temperature sulfides (Jenner et al., 2012). The sulfides then break down during subduction and release these elements into the mantle wedge (Noll et al., 1996). The formation of hydrothermal sulfides seems to be the best way to concentrate the elements that are enriched in KI, but these sulfides would need to survive subduction to be incorporated into the KI source.

Ireland et al. (2009) found that W enrichments in several Hawaiian basalts could be explained by the mixing of 3–20% recycled oceanic crust and sediments into a depleted mantle source. Pursuing this hypothesis further, we modeled the source composition for the Kilauea Iki picrites to understand the origin of these enrichments.

6.6. The Kilauea mantle source

The Hawaiian mantle source is heterogeneous, as reflected in many trace element and isotopic studies of lavas from difference volcanic centers (Jackson et al., 2012, and references therein). Multiple mantle sources have been invoked to explain these differences: the EM1 signature in Hawaii may reflect a primitive mantle source, given Sr, Pb, and Nd isotopic signatures (White, 1985), while others consider the mantle source to be a mixture of a more depleted reservoir and recycled oceanic crust (White and Hofmann, 1982). Indeed, Pietruszka et al. (2013) found that the Kilauea source can be explained by the addition of 8–16% hydrothermally altered oceanic crust, while Ireland et al. (2009) concluded that the source is composed of depleted MORB mantle with the addition of 3–20% recycled oceanic crust and terrigeneous sediments. Here we explore both a primitive mantle source and a source influenced by recycled crust to explain the Cu, Ga, Ge, As, Mo, Ag, Cd, In, Sn, Sb, W, Tl, Pb, and Bi abundances in Kilauea Iki.

The enrichment of chalcophile PGEs in KI (Pitcher et al., 2009) suggests that sulfides in the mantle source were exhausted by partial melting. Modeling of Pietruszka and Garcia (1999) and Pietruszka et al. (2006) suggest that Kilauea basalts represent 10% partial melt of the mantle source, while Ireland et al. (2009) infer 5–10% partial melting of the mantle. Interestingly, neither of these estimates are high enough for sulfides to be consumed by partial melting, which occurs at 12–16% partial melting of a depleted mantle source (Luguet et al., 2003; Nielsen et al., 2014). Thus, we calculated the Kilauea source abundance for Cu, Ga, Ge, As, Mo, Ag, Cd, In, Sn, Sb, W, Tl, Pb, and Bi using the batch melting equation $C_o = C_l(D + (1 - D) * F)$ and a 12% melt fraction – the minimum melt fraction theorized to exhaust sulfides from the mantle source. Element abundances in the KI primitive magma composition (C_l) were calculated at 15 wt% MgO

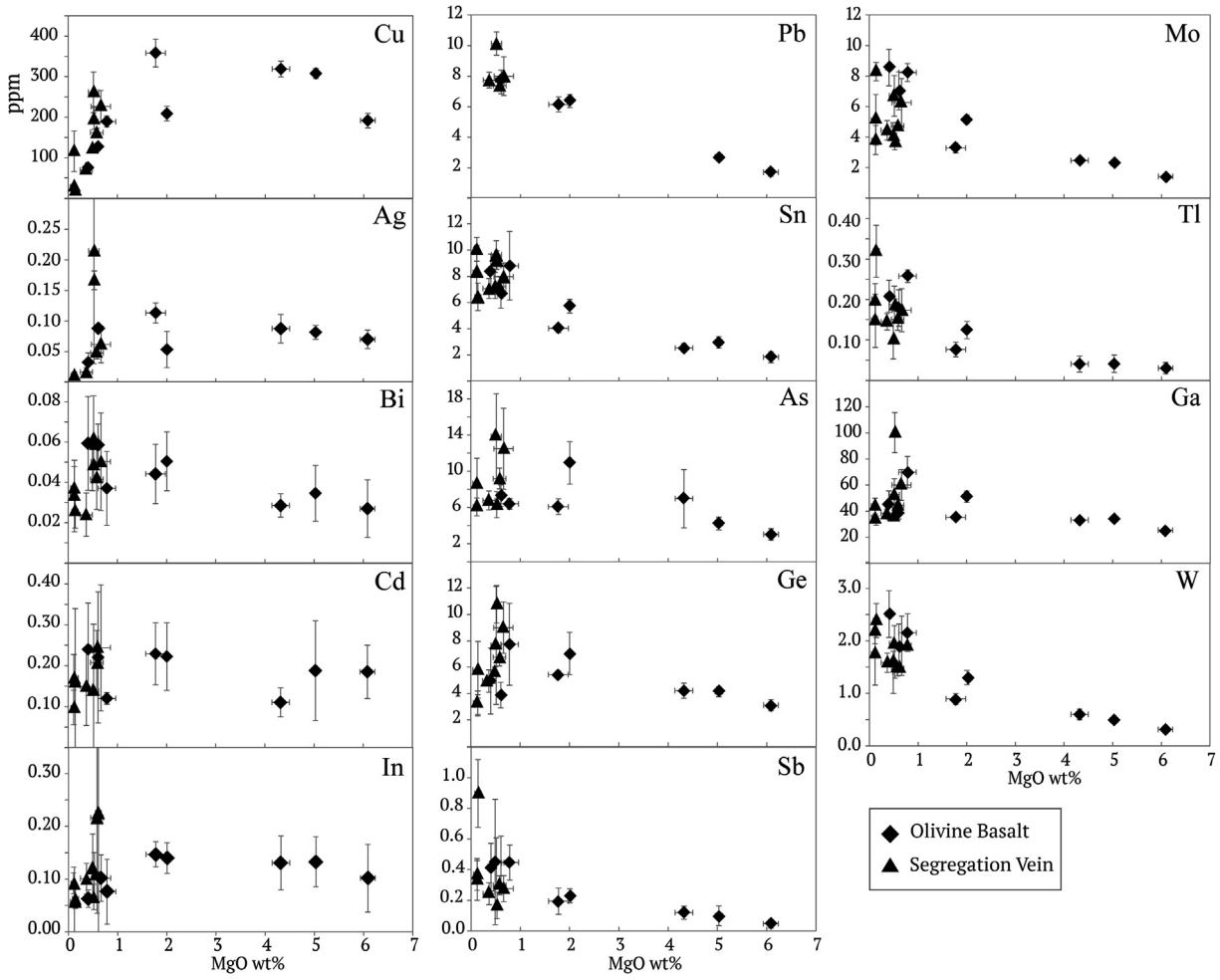

Fig. 4. Glass MgO variation diagrams displaying trace element differentiation patterns. All trace elements are reported in ppm. Each point represents a sample average of 6–10 laser ablation point analyses. Error bars represent 1σ of the mean of replicate analyses.

by fitting a linear regression through MgO variation diagrams of whole rock data for the drill core picrites and basalts (26–7 wt% MgO_{WR}) and olivine, as this is the fractionating phase on the control line, per Puchtel et al. (2004) (supplementary figures). Cerium and Er were also added to the model as a check for accuracy, given the predictable behavior of LREE and HREE during mantle melting. Because Cd and Bi abundances in volcanic glasses have been shown to be affected by outgassing, the calculated primitive magma composition may be incorrect for these elements. They are included in the calculations, but the results should be viewed with caution. Model details including bulk D values and source modal mineralogy are included in the supplementary figures and tables.

The model results are shown in Fig. 7. While the calculated KI mantle source composition is within error of the primitive mantle estimate for some elements, In, Mo, and LREE (as indicated by Ce), are too enriched in the KI source to be derived solely from a primitive mantle source. Incorporation of a UCC component (carried in terrigenous sediment) produces a better fit to the data. When the elements are ordered on a spider diagram by their relative abundance in primitive KI magmas relative to primitive MORB (Jenner and O'Neill, 2012), as calculated by $(X_{KI} - X_{MORB})/X_{MORB}$. With the exception of Ag, the more enriched KI elements that plot at the left side of the diagram correspond quite well with elements that are more enriched in the UCC (Fig. 8). The general trend suggests incorporation of recycled UCC-derived sediments in the mantle source of KI. Therefore, we modelled the KI source as a mixture of depleted MORB mantle (DMM) source and a recycled crust package composed of MORB + UCC sediments per Ireland et al. (2009) to better explain the trace element signature of Kilauea (Fig. 9, model details in supplement). We find that the calculated KI source composition matches this DMM + 10–20% recycled crust source, within error, for all elements analyzed here (Fig. 9). Specifically, the abundances of the elements In, Mo, Ag, Ce, Sn, Cd, Sb, Bi, W, and As, that are 1.5–4 times more enriched in the KI source than in the primitive mantle, are much better explained by the addition of around 20% MORB and UCC-derived sediments to DMM than by a pure primitive mantle source (see the supplement for a discussion of the possible influence of subduction on these elements).

We conclude that the enrichments observed in the Kilauea Iki magmas (Fig. 6) and the calculated KI mantle

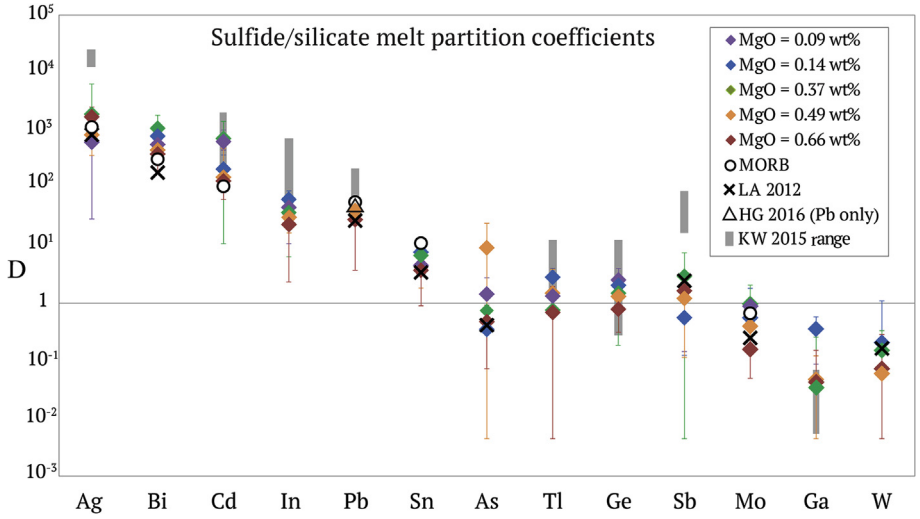

Fig. 5. Partition coefficients measured in five KI samples (colored diamonds). Error bars represent 2 standard deviations of the mean of multiple sulfide-silicate analyses per sample. The different colored diamonds represent KI glasses with different MgO contents, as labelled in the symbol key; purple diamond corresponds to sulfides in sample 75-1-125.0, blue is 81-1-169.9, green is 79-3-158.0, orange is 67-3-75.7, and red is 67-3-76.2. The mean glass composition for each sample was used to calculate the D values. Average $D^{\text{sulfide liquid/silicate melt}}$ values from Li and Audétat (2012) at FMQ > 0 are represented by an X. MORB values from Patten et al. (2013) are represented by open circles and Pb values expected in MORB, as measured by Hart and Gaetani (2016), is represented with a triangle. Cu is not plotted because it is a main structural component to the sulfides. The gray bar represents the range of $D^{\text{sulfide/silicate}}$ that were calculated using the Kiseeva and Wood (2015) equation at 1050 °C, average Cu (45 wt%) and Ni (0.7 wt%) abundances, and FeO content of the silicate melt between 7.3 and 1.3 wt%. (For interpretation of the references to color in this figure legend, the reader is referred to the web version of this article.)

source trace element signature can be explained by mixing of 10–20% recycled crust composed of 95–99% is MORB and 1–5% is UCC-derived sediments. These calculations agree with the results of other studies: Ireland et al. (2009) found the Hawaiian mantle source may contain 3–20% recycled material, Sobolev et al. (2005) – 12% recycled material; and Pietruszka et al. (2013) – 9–16% recycled material.

6.7. Behavior of chalcophile elements in the mantle

The excellent agreements between the partition coefficients calculated in this study and those calculated for sulfide blebs in MORB, as well as the data for multiple experimental partitioning studies demonstrate that Ag, Bi, Cd, and In will behave as strongly chalcophile elements regardless of sulfide composition or tectonic setting. Unsurprisingly, Wang and Becker (2015) find that Cu and Ag behave as chalcophile elements in mantle pyroxenites and they infer limited fractionation during melt extraction from the upper mantle. Lead and Sn may behave as chalcophile elements in the mantle as they do in KI, but this is more speculative as sulfides do not entirely control their behavior in KI.

In contrast to above results and D values measured in MORB for Cd and In (Patten et al., 2013), Witt-Eickshen et al. (2009) found, in a laser ablation ICP-MS study of peridotite xenoliths, that Ga, Cd, In, and Sn are hosted primarily in silicates rather than sulfides. Although sulfide concentrations of In and Sn were greater than those of coexisting silicates, the very low abundance of sulfides (found as a minor phase in only two samples from Kilbourne Hole, out of 24 samples investigated) made sulfides insignificant to the whole rock mass balance. Based on these results, and the fact that they could achieve whole rock mass balance for all of these elements without sulfides, they suggested that Ga, Cd, In, and Sn behave as lithophile elements in the lithospheric mantle. Of the suite of nominally chalcophile elements they analyzed, only As was found to enter sulfide in significant amounts.

If the conclusion of Witt-Eickshen et al. (2009) hold, it suggests there is a significant difference in the partitioning of Cd, In, and Sn between sulfide and silicate in peridotitic versus basaltic to intermediate systems. However, sulfides are generally poorly preserved in xenolithic peridotites due to their breakdown post-eruption (e.g., through circulation of meteoric water, Lorand, 1990) or during interaction with sulfide undersaturated melts and/or fluids in the mantle shortly before xenolith entrainment (Liu et al., 2010; Harvey et al., 2015). If elements originally contained within the sulfides are lost from the whole rock upon sulfide breakdown (as has been demonstrated for S, Se, Os, Pd, and Re, Lorand, 1990; Handler et al., 1999; Liu et al., 2010; Harvey et al., 2015), then whole rock concentrations do not reflect the concentration of the mantle, and inferences about these elements' geochemical behavior based on whole rock mass balance like that undertaken by Witt-Eickshen et al. (2009) may be erroneous.

Using the partitioning equation of Kiseeva and Wood (2015) and a wide range of sulfide compositions, we find that D_{Cd} never falls below 1, and the only conditions that would generate D_{In} below one have $Ni_{sulfide} \geq 50$ wt%, $FeO_{silicatemelt} \geq 22$ wt%, and $T \geq 1300$ °C, simultaneously. This scenario would not occur in the lithospheric mantle.

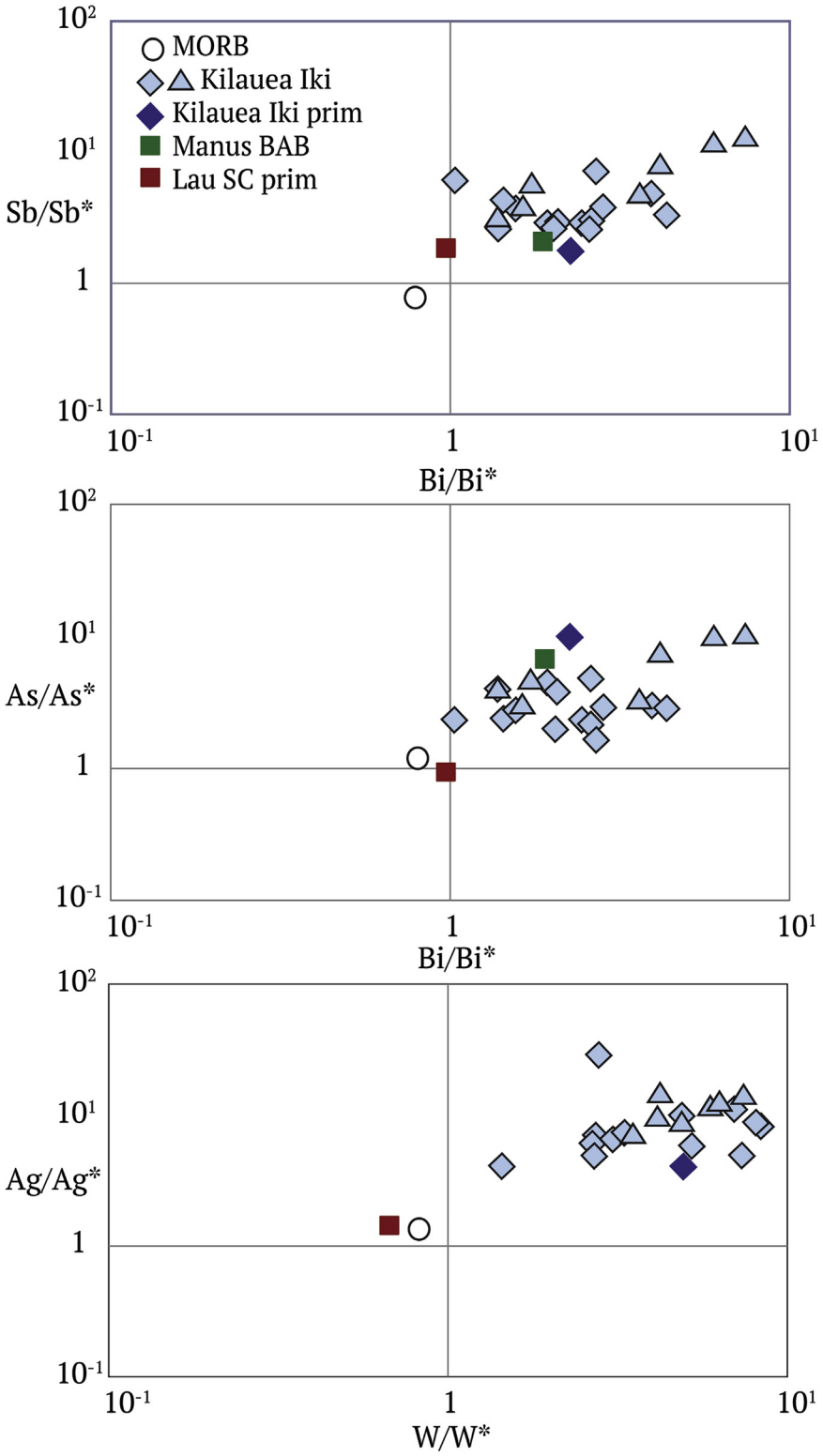

Fig. 6. Enrichments observed in Kilauea Iki lavas. Each element is normalized to an interpolated value (denoted with a star), which is the expected concentration of that element if it partitions the same as similarly compatible elements, as observed in MORB. This is calculated as Sb^*, Bi^*, and $As^* = (V \times Cd)^{0.5}$, Ag^* and $W^* = (Cu \times Ge)^{0.5}$. Average MORB (Jenner and O'Neill, 2012) is represented with an open circle, all measured values in Kilauea samples are in light blue diamonds (basalts) and triangles (segregation veins), primitive Kilauea is a dark blue diamond, primitive Eastern Manus Back-arc basin (Jenner et al., 2012) in a green square, and primitive Northwestern Lau Spreading Center (Jenner et al., 2012) is in a red square. (For interpretation of the references to color in this figure legend, the reader is referred to the web version of this article.)

Table 7
Average partition coefficients ($D^{silicate/glass}$) calculated for the silicates olivine and augite. Complete trace element and partition coefficient data is listed in the appendix Table A5.

	Cu	Ga	Ge	As	Mo	Ag	Cd
olivine	**0.10**	**0.01**	**0.34**	**0.01**	**0.03**	**0.06**	**0.83**
2s	0.08	0.00	0.03	0.01	0.06	*1 analysis*	
augite	**0.21**	**0.04**	**0.30**	**0.04**	**0.01**	**bdl**	**0.34**
2s	0.21	0.04	0.30	0.04	0.01		0.34

In	Sn	Sb	W	Tl	Pb	Bi
0.14	**0.02**	**0.02**	**bdl**	**bdl**	**bdl**	**0.27**
0.16	0.01	*1 analysis*				
0.11	**0.00**	**bdl**	**bdl**	**bdl**	**bdl**	**bdl**
0.11	0.00					

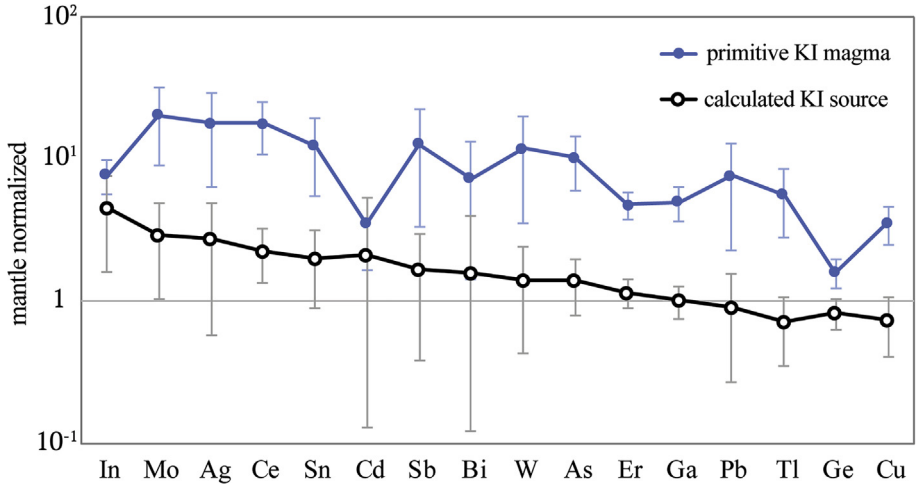

Fig. 7. Trace element diagram normalized to primitive mantle (McDonough and Sun, 1995) showing the estimated KI primitive magma composition, calculated at 15 wt% MgO given a linear regression through whole rock data in blue. The mantle source results from the batch melting calculations are shown in black, open circles. Error bars represent 2σ calculated from the least squares regression. Cadmium and Bi whole rock data showed virtually no correlation between 25 wt% and 10 wt% MgO (supplementary figures), so their estimated primitive abundance has a large error associated with it. Additionally, Cd and Bi may have been affected by degassing. The elements are ordered by their abundance in the calculated mantle source. (For interpretation of the references to color in this figure legend, the reader is referred to the web version of this article.)

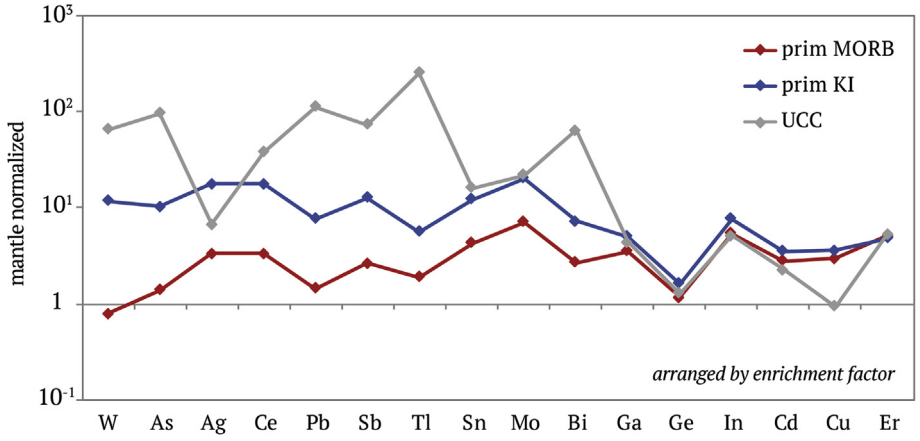

Fig. 8. Trace element diagram normalized to primitive mantle (McDonough and Sun, 1995) showing the same primitive KI magma as plotted in Fig. 7 (blue circles) as well as primitive MORB (Jenner and O'Neill, 2012) in red triangles and UCC (Rudnick and Gao, 2014) abundance in gray diamonds. Elements are ordered by the relative difference between their abundance in the primitive KI and primitive MORB calculated as $(X_{KI} - X_{MORB})/X_{MORB}$. Note that, with the exception of Ag, the elements that are more enriched in KI are also quite abundant in the UCC. (For interpretation of the references to color in this figure legend, the reader is referred to the web version of this article.)

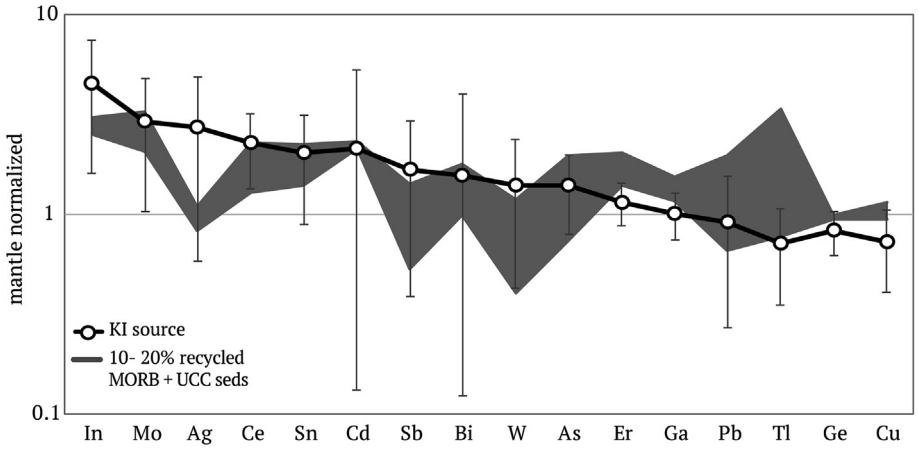

Fig. 9. Trace element diagram, normalized to primitive mantle (McDonough and Sun, 1995) showing the results of the mantle mixing calculations (gray region) and Kilauea mantle source calculation (black line). The gray region represents a range of materials mixed into a DMM source from 10% recycled material of which 99% is MORB and 1% are sediments derived from the UCC (low end) to 20% recycled material of which 95% is MORB and 5% are UCC sediments (high end). All element concentrations agree within error between the modeled KI source and mantle mixture region. Cadmium and Bi may have been affected by degassing, so their mantle abundances may represent minima.

We therefore conclude that, like Cu and Ag (Wang and Becker, 2015), Cd, In and possibly Sn are very likely chalcophile in the mantle lithosphere. Inferences regarding the primitive mantle content of these chalcophile elements should be re-examined using peridotites that have not experienced sulfide breakdown.

7. CONCLUSIONS

In the Kilauea Iki lava lake Ag, Bi, Cd, In, Pb, and Sn are chalcophile, As, Ge, Sb, and Tl are weakly chalcophile to lithophile, and Mo, Ga, and W are lithophile. The mean $D^{\text{sulfide/silicate}}$ are: $D_{Ag} = 1252 \pm 1201$ (2σ), $D_{Bi} = 663 \pm 576$, $D_{Cd} = 380 \pm 566$, $D_{In} = 40 \pm 34$, $D_{Pb} = 34 \pm 18$, $D_{Sn} = 5.3 \pm 3.6$, $D_{As} = 2.4 \pm 7.6$, $D_{Ge} = 1.6 \pm 1.4$, $D_{Sb} = 1.3 \pm 1.5$, $D_{Tl} = 1.1 \pm 1.7$, $D_{Mo} = 0.56 \pm 0.6$, $D_{Ga} = 0.10 \pm 0.3$, and $D_{W} = 0.11 \pm 0.1$. The chalcophile elements can be further subdivided into strongly chalcophile elements (Ag, Bi, Cd, and In), whose differentiation behavior is entirely controlled by sulfide saturation, and moderately chalcophile elements (Pb and Sn) that partition into sulfides but do not significantly fractionate from the melt after sulfide saturation given their low $D^{\text{sulfide/silicate}}$ values and the low volume of sulfides. These findings are consistent with results from a study of MORB sulfides (Patten et al., 2013), as well as experimental studies run at conditions similar to those that are found in KI (Li and Audétat, 2012; Kiseeva and Wood, 2013). Gallium, Ge, and As may partition into apatite where they could substitute for P, however they likely also partition into aluminosilicate phases where they substitute for Al and Si. Antimony, Tl, and W behave as incompatible elements during differentiation.

Molybdenum generally behaves as a lithophile element; it is not primarily concentrated in the sulfides and is instead found in the glass and Fe-Ti oxides where Mo^{6+} may substitute for Ti^{4+}. This has implications for the removal of Mo from the Archean continental crust: common igneous sulfides (whose breakdown rate is a function of atmospheric oxygen levels) are not a significant host of Mo, whereas glass (which can readily break down in the absence of atmospheric oxygen) is a significant host of Mo.

The Kilauea mantle source is modeled as a mixture of depleted MORB mantle (DMM) and a recycled package of crust containing MORB and UCC derived sediments. The abundances of the elements studied here are best explained by the addition of 10–20% recycled oceanic crust (of which 1–5% is UCC-derived sediments) to DMM. The partial melting of this UCC-influenced source can explain the apparent enrichments in As, Ag, Sb, W, and Bi and other elements observed in Kilauea relative to MORB.

ACKNOWLEDGEMENTS

This work was supported by the University of Maryland and National Science Foundation grant EAR 133810 (A. Anbar, PI, R.L. Rudnick, co-I). Frances Jenner is thanked for discussion on analytical methods. We are grateful for comments from Cin-Ty Lee and reviews from Kate Kiseeva, Igor Puchtel, an anonymous reviewer, and editor Marc Norman.

APPENDIX A. SUPPLEMENTARY MATERIAL

Supplementary data associated with this article can be found, in the online version, at http://dx.doi.org/10.1016/j.gca.2017.04.033.

REFERENCES

Anbar A. D., Duan Y., Lyons T. W., Arnold G. L., Kendall B., Creaser R. A., Kaufman A. J., Gordon G. W., Scott C., Garvin J. and Buick R. (2007) A whiff of oxygen before the great oxidation event? *Science* **317**, 1903–1906.

Arevalo R. and McDonough W. F. (2008) Tungsten geochemistry and implications for understanding the Earth's interior. *Earth Planet. Sci. Lett.* **272**, 656–665.

Audétat A., Dolejs D. and Lowenstern J. B. (2011) Molybdenite saturation in silicic magmas: occurrence and petrological implications. *J. Petrol.* **52**(5), 891–904.

Cawood P. A., Hawkesworth C. J. and Dhuime B. (2013) The continental record and the generation of continental crust. *GSA Bull.* **125**, 14–32.

Chen H., Savage P., Teng F. Z., Helz R. T. and Moynier F. (2013) Zinc isotope fractionation during magmatic differentiation and the isotopic composition of the bulk Earth. *Earth Planet. Sci. Lett.* **369–370**, 34–42.

Condie K. C. (1993) Chemical composition and evolution of the upper continental crust: constraining results from surface samples and shales. *Chem. Geol.* **104**, 1–37.

Erickson B. E. and Helz G. R. (2000) Molybdenum (VI) speciation in sulfidic waters: stability and lability of thiomolybdates. *Geochim. Cosmochim. Acta* **64**, 1149–1158.

Gaschnig R. M., Rudnick R. L. and McDonough W. F. (2015) Determination of Ga, Ge, Mo, Ag, Cd, In, Sn, Sb, W, Tl and Bi in USGS whole-rock reference materials by standard addition ICP-MS. *Geostan. Geoanal. Res.* **39**, 371–379.

Gaschnig R. M., Rudnick R. L., McDonough W. F., Kaufman A. J., Valley J. W., Gao S. and Beck M. (2016) Compositional evolution of the upper continental crust through time, as constrained by ancient glacial diamictites. *Geochim. Cosmochim. Acta* **186**, 316–343.

Ghiorso M. S. and Evans B. W. (2008) Thermodynamics of rhombohedral oxide solid solutions and a revision of the Fe-Ti two-oxide geothermometer and oxygen-barometer. *Am. J. Sci.* **208**, 957–1039.

Goldschmidt V. M. (1937) *The Principles of Distribution of Chemical Elements in Minerals and Rocks*. Hugo Müller Lecture, Chemical Society.

Gregory D. D., Large R. L., Halpin J. A., Bauturina E. L., Lyons T. W., Wu S., Danyushevsky L., Sack P. J., Chappaz A., Maslennikov V. V. and Bull S. W. (2015) Trace element content of sedimentary pyrite in black shales. *Econ. Geol.* **110**, 1389–1410.

Helz R. T. and Taggert J. E. (2010) *Whole-rock analyses of core samples from the 1988 drilling of Kilauea Iki Lava Lake, Hawaii, USGS Open File Report 2010–1093*.

Hart S. R. and Gaetani G. A. (2006) Mantle Pb paradoxes: the sulfide solution. *Contrib. Mineral. Petrol.* **152**, 295–308.

Hart S. R. and Gaetani G. A. (2016) Experimental determination of Pb partitioning between sulfide melt and basalt melt as a function of P, T, and X. *Geochim. Cosmochim. Acta* **185**, 9–20.

Harvey J., Konig S. and Luguet A. (2015) The effects of melt depletion and metasomatism on highly siderophile and strongly chalcophile elements: S-Se-Te-Re-PGE systematics of peridotite xenoliths from Kilbourne Hole, New Mexico. *Geochim. Cosmochim. Acta* **166**, 210–233.

Helmy H. M., Ballhaus C., Wohlgemuth-Ueberwasser C., Fonseca R. O. C. and Laurenz V. (2010) Partitioning of Se, As, Sb, Te and Bi between monosulfide solid solution and sulfide melt – application to magmatic sulfide deposits. *Geochim. Cosmochim. Acta* **74**, 6174–6179.

Helz R. T. (1987) Differentiation behavior of Kilauea Iki lava lake, Kilauea Volcano, Hawaii: an overview of past and current work. In *Magmatic Processes: Physicochemical Principles*, vol. 1 (ed. B. O. Mysen). Geochemical Society Special Publication, pp. 241–258.

Helz R. T. (2012) *Trace Element Analyses of Core Samples from the 1967-1988 Drillings of Kilauea Iki Lava Lake, Hawaii. USGS Open-file Report 2012-1050*.

Helz R. T. and Wright T. L. (1983) *Drilling report and core logs for the 1981 drilling of Kilauea Iki lava lake (Kilauea Volcano, Hawaii), with comparative notes on earlier (1967–1979 drilling experiences. USGS Open-file Report 83-326*.

Helz R. T. and Thornber C. R. (1987) Geothermometry of Kilauea Iki Lava Lake, Hawaii. *Bull. Volcanol.* **49**, 651–668.

Helz R. T. and Wright T. L. (1992) Differentiation and magma mixing on Kilauea's east zone. *Bull. Volcanol.* **54**, 361–384.

Helz R. T., Kirschenbaum H., Marinenko J. M. and Qian R. (1994) *Whole-rock analyses of core samples from the 1967, 1975, 1979 and 1981 drillings of Kilauea Iki lava lake, Hawaii. USGS Open-file Report 94-684*.

Helz G. R., Bura-Nakic E., Mikac N. and Ciglenecki I. (2011) New model for molybdenum behavior in euxinic waters. *Chem. Geol.* **284**, 323–332.

Helz R. T., Cottrell E., Brounce M. N. and Kelley K. A. (2017) Olivine-melt relationships and syneruptive redox variations in the 1959 eruption of Kilauea Volcano as revealed by XANES. *J. Volcanol. Geotherm. Res.*. http://dx.doi.org/10.1016/j.volgeores.2016.12.006.

Hofmann A. W. (1988) Chemical differentiation of the Earth: the relationship between mantle, continental crust, and oceanic crust. *Earth Planet Sci. Lett.* **90**, 297–314.

Hofmann A. W. (2003) Sampling mantle heterogeneity through oceanic basalts: isotopes and trace elements. *Treat. Geochem.* **2** (03), 61–101.

Ireland T. J., Arevalo R., Walker R. J. and McDonough W. F. (2009) Tungsten in Hawaiian picrites: a compositional model for the sources of Hawaiian lavas. *Geochim. Cosmochim. Acta* **73**, 4517–4530.

Jackson M. G., Weis D. and Huang S. (2012) Major element variations in Hawaiian shield lavas: source features and perspectives from global ocean island basalt (OIB) systematics. *Geochem. Geophys. Geosyst.* **13**, 1–24.

Jenner F. E. and O'Neill H. S. C. (2012) Analysis of 60 elements in 616 ocean floor basaltic glasses. *Geochem. Geophys. Geosyst.* **13** (1), 1–11.

Jenner F. E., O'Neill H. S. C., Arculus R. J. and Mavrogenes J. A. (2010) The magnetite crisis in the evolution of arc-related magmas and the initial concentration of Au, Ag, and Cu. *J. Petrol.* **51**, 2445–2464.

Jenner F. E., Arculus R. J., Mavrogenes J. A., Dyriw N. J., Nebel O. and Hauri E. H. (2012) Chalcophile element systematics in volcanic glasses from the northwestern Lau Basin. *Geochem. Geophys. Geosyst.* **13**(6), 1–25.

Jenner F. E., Hauri E. H., Bullock E. S., Koenig S., Arculus R. J., Mavrogenes J. A., Mikkelson N. and Goddard C. (2015) The competing effects of sulfide saturation versus degassing on the behavior of the chalcophile elements during the differentiation of hydrous melts. *Geochem. Geophys. Geosyst.* **16**, 1490–1507.

Jochum K. P. and Hofmann A. W. (1997) Constraints on earth evolution from antimony in mantle-derived rocks. *Chem. Geol.* **139**, 39–49.

Jochum K. P., Hofmann A. W. and Seufert H. M. (1993) Tin in mantle-derived rocks: constraints on Earth evolution. *Geochim. Cosmochim. Acta* **57**, 3585–3595.

Jugo P. (2009) Sulfur content at sulfide saturation in oxidized magmas. *Geology* **37**(5), 415–418.

Kato C., Moynier F., Foriel J., Teng F. Z. and Puchtel I. S. (2017) The gallium isotopic composition of the bulk silicate Earth. *Chem. Geol.* **448**, 164–172.

Kiseeva E. S. and Wood B. J. (2013) A simple model for chalcophile elements partitioning between sulphide and silicate liquids with geochemical applications. *Earth Planet. Sci. Lett.* **383**, 68–81.

Kiseeva E. S. and Wood B. J. (2015) The effects of composition and temperature on chalcophile and lithophile element partitioning into magmatic sulphides. *Earth Planet. Sci. Lett.* **424**, 280–294.

Korzhinsky M. A., Tkachenko S. I., Shmulovich K. I., Taran Y. A. and Steinberg G. S. (1994) Discovery of a pure rhenium mineral at Kudriavy volcano. *Nature* **369**, 51–52.

Kuroda P. K. and Sandell E. B. (1954) Geochemistry of Molybdenum. *Geochim. Cosmochim. Acta* **6**, 35–63.

Lassiter J. C. (2003) Rhenium volatility in subaerial lavas: constraints from subaerial and submarine portions of the HDSP-2 Mauna Kea drillcore. *Earth Planet. Sci. Lett.* **214**, 311–325.

Lee C. T. A., Luffi P., Chin E. J., Bouchet R., Dasgupta R., Morton D. M., Le Roux V., Yin Q. and Jin D. (2012) Copper systematics in arc magmas and implications for crust-mantle differentiation. *Science* **336**, 64–68.

Li Y. and Audétat A. (2012) Partitioning of V, Mn Co, Ni, Cu, Zn, As, Mo, Ag, Sn, Sb, W, Au, Pb, and Bi between sulfide phases and hydrous basanite melt at upper mantle conditions. *Earth Planet. Sci. Lett.* **335–336**, 327–340.

Li Y. and Audétat A. (2015) Effects of temperature, silicate melt composition, and oxygen fugacity on the partitioning of V, Mn Co, Ni, Cu, Zn, As, Mo, Ag, Sn, Sb, W, Au, Pb, and Bi between sulfide phases and silicate melt. *Geochim. Cosmochim. Acta* **162**, 25–45.

Liu J., Rudnick R. L., Walker R. J., Gao S., Wu F. and Piccoli P. M. (2010) Processes controlling highly siderophile element fractionations in xenolithic peridotites and their influence on Os isotopes. *Earth Planet. Sci. Lett.* **297**, 287–297.

Lorand J. P. (1990) Are spinel lherzolite xenoliths representative of the abundance of sulfur in the upper mantle? *Geochim. Cosmochim. Acta* **54**, 1487–1492.

Luguet A., Lorand J. P. and Seyler M. (2003) Sulfide petrology and highly siderophile element geochemistry of abyssal peridotites: A coupled study of samples from the Kane Fracture Zone (45° W 23°20N, MARK Area, Atlantic Ocean). *Geochim. Cosmochim. Acta* **67**, 1553–1570.

McDonough W. F. and Sun S. s. (1995) The composition of the Earth. *Chem. Geol.* **120**, 223–253.

Miller K. J., Zhu W. L., Montesi L. G. J. and Gaetani G. A. (2014) Experimental quantification of permeability of partially molten mantle rock. *Earth Planet. Sci. Lett.* **388**, 273–282.

Mungall J. E. and Brenan J. M. (2014) Partitioning of platinum-group elements and Au between sulfide liquid and basalt and the origins of mantle-crust fractionation of the chalcophile elements. *Geochim. Cosmochim. Acta* **125**, 265–289.

Newsom H. E. and Palme H. (1984) The depletion of siderophile elements in the Earth's mantle: new evidence from molybdenum and tungsten. *Earth Planet. Sci. Lett.* **69**, 354–364.

Nielsen S. G., Shimizu N., Lee C. T. A. and Behn M. D. (2014) Chalcophile behavior of thallium during MORB melting and implications for the sulfur content of the mantle. *Geochem. Geophys. Geosyst.* **15**, 1–15.

Noll P. D., Newsom H. E., Leeman W. P. and Ryan J. G. (1996) The role of hydrothermal fluids in the production of subduction zone magmas: Evidence from siderophile and chalcophile trace elements and boron. *Geochim. Cosmochim. Acta* **60**, 587–611.

Norman M. D., Garcia M. O. and Bennett V. C. (2004) Rhemium and chalcophile elements in basaltic glasses from Ko'olau and Moloka'I volcanoes: magmatic outgassing and composition of the Hawaiian plume. *Geochim. Cosmochim. Acta* **68**, 3761–3777.

O'Neill H. S. C. and Eggins S. M. (2002) The effect of melt composition on trace element partitioning; and experimental investigation of the activity coefficients of FeO, NiO, CoO, MoO_2 and MoO_3 in silicate melts. *Chem. Geol.* **186**, 151–181.

Patten C., Barnes S., Mathez E. A. and Jenner F. E. (2013) Partition coefficients of chalcophile elements between sulfide and silicate melts and the early crystallization history of sulfide liquid: LA-ICP-MS analysis of MORB sulfide droplets. *Chem. Geol.* **358**, 170–188.

Paton C., Hellstrom J., Paul B., Woodhead J. and Hergt J. (2011) Iolite: freeware for the visualisation and processing of mass spectrometric data. *J. Anal. Atom. Spectrom.* **26**, 2508–2518.

Peach C. L., Mathez E. A. and Keays R. R. (1990) Sulfide melt-silicate melt distribution coefficients for noble metals and other chalcophile elements as deduced from MORB: implications for partial melting. *Geochim. Cosmochim. Acta* **54**, 3379–3389.

Pietruszka A. J. and Garcia M. O. (1999) A rapid fluctuation in the mantle source and melting history of Kilauea Volcano inferred from the geochemistry of its historical summit lavas (1790–1982). *J. Petrol.* **40**, 1321–1342.

Pietruszka A. J., Hauri E. K., Carlson R. W. and Garcia M. O. (2006) Remelting of recently depleted mantle within the Hawaiian plume inferred from the 226Ra-230^{Th}-238U disequilibria of Pu'u 'O'o eruption lavas. *Earth Planet. Sci. Lett.* **244**, 155–169.

Pietruszka A. J., Norman A. D., Garcia M. O., Marske J. P. and Burns D. H. (2013) Chemical heterogeneity in the Hawaiian mantle plume from the alteration and dehydration of recycled oceanic crust. *Earth Planet. Sci. Lett.* **361**, 298–309.

Pitcher L., Helz R. T., Walker R. J. and Piccoli P. M. (2009) Fractionation of the platinum-group elements and Re during crystallization of basalt in Kilauea Iki Lava Lake, Hawaii. *Chem. Geol.* **260**, 196–210.

Prytulak J., Nielsen S. G., Plank T., Barker M. and Elliot T. (2013) Assessing the utility of thallium and thallium isotopes for tracing subduction zone inputs to the Mariana arc. *Chem. Geol.* **345**, 139–169.

Puchtel I. S., Humayun M., Campbell A. J., Sproule R. A. and Lesher C. M. (2004) Platinum group element geochemistry of komatiites from the Alexo and Pyke Hill areas, Ontario, Canada. *Geochim. Cosmochim. Acta* **68**, 1361–1383.

Richter D. H. and Moore J. G. (1966) *Petrology of the Kilauea Iki Lava Lake, Hawaii, USGS. Professional Paper 537-B*.

Rudnick R. L. and Gao S. (2014) Composition of the continental crust. *Treat. Geochem.* **3**, 1–64 (second ed.).

Savage P. S., Moynier F., Chen H., Shofner G., Siebert J. and Puchtel I. S. (2015) Copper isotope evidence for large-scale sulphide fractionation during Earth's differentiation. *Geochem. Perspect. Lett.* **1**, 53–64.

Scott C., Lyons T. W., Bekker A., Shen Y., Poulton S. W., Chu X. and Anbar A. D. (2008) Tracing the stepwise oxygenation of the Proterozoic ocean. *Nature* **452**, 456–459.

Sobolev A. V., Hofmann A. W., Sobolev S. V. and Kikogosian I. K. (2005) An olivine-free mantle source of Hawaiian shield basalts. *Nature* **434**, 590–597.

Stone W. E. and Fleet M. E. (1991) Nickel-copper sulfides from the 1959 eruption of Kilauea Volcano, Hawaii: contrasting compositions and phase relations in eruption pumice and Kilauea Iki lava lake. *Am. Mineral.* **76**, 1363–1372.

Sun W., Bennett V. C., Eggins S. M., Kamenetsky V. S. and Arculus J. (2003) Enhanced mantle to crust rhenium transfer in undegassed arc magmas. *Nature* **422**, 294–297.

Tang M., Chen K. and Rudnick R. L. (2016) Archean upper crust transition from mafic to felsic marks the onset of plate tectonics. *Science* **351**, 372–375.

Taylor S. R. and McLennan S. M. (1985) *The Continental Crust; Its Composition and Evolution*. Blackwell, Oxford.

Teng F. Z., Wadhwa M. and Helz R. T. (2007) Investigation of magnesium isotope fractionation during basalt differentiation: implications for a chondritic composition of the terrestrial mantle. *Earth Planet. Sci. Lett.* **261**, 84–92.

Teng F. Z., Dauphas N. and Helz R. T. (2008) Iron isotope fractionation during magmatic differentiation in Kilauea Iki Lava Lake. *Science* **320**, 1620–1622.

Tessalina S. G., Yudovskaya M. A., Chaplygin I. V., Birck J. and Capmas F. (2008) Sources of unique rhenium enrichments in fumaroles and sulphides at Kudryavy volcano. *Geochim. Cosmochim. Acta* **72**, 889–909.

Tomascak P. B., Tera F., Helz R. T. and Walker R. J. (1999) The absence of lithium isotope fractionation during basaltic differentiation: new measurements by multicollector sector ICP-MS. *Geochim. Cosmochim. Acta* **63**(6), 907–910.

Walker R. J. (2016) Siderophile elements in tracing planetary formation and evolution. *Geochem. Perspect.* **5**(1), 1–143.

Wang and Becker (2015) Abundances of Ag and Cu in mantle peridotites and the implications for the behavior of chalcophile elements in the mantle. *Geochim. Cosmochim. Acta* **160**, 209–226.

White W. M. (1985) Sources of oceanic basalts: radiogenic isotopic evidence. *Geology* **13**, 115–118.

White W. M. and Hofmann A. W. (1982) Sr and Nd isotope geochemistry of oceanic basalts and mantle evolution. *Nature* **296**, 821–825.

Wright T. L. (1973) Magma mixing as illustrated by the 1959 eruption. *Kilauea Volcano, Hawaii: Geol. Soc. Am. Bull.* **84**, 849–858.

Witt-Eickshen G., Palme H., O'Neill H. S. C. and Allen C. M. (2009) The geochemistry of the volatile trace elements As, Cd, Ga, In, and Sn in the Earth's mantle: new evidence from in situ analyses of mantle xenoliths. *Geochim. Cosmochim. Acta* **73**, 1755–1778.

Yang J., Siebert C., Barling J., Savage P., Liang Y. and Halliday A. N. (2015) Absence of molybdenum isotope fractionation during magmatic differentiation at Hekla volcano, Iceland. *Geochim. Cosmochim. Acta* **162**, 126–136.

Yi W., Halliday A. N., Alt J. C., Lee D., Rehkamper M., Garcia M. O., Langmuir C. H. and Su Y. (2000) Cadmium, indium, tin, tellurium, and sulfur in oceanic basalts: implications for chalcophile element fractionation in the Earth. *J. Geophys. Res.* **105**, 18927–18948.

Associate editor: Marc Norman

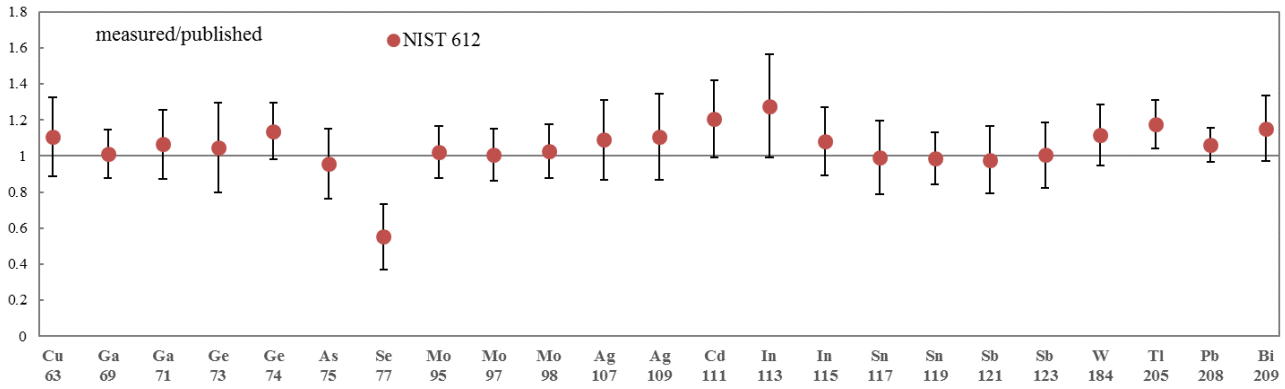

Figure A-NIST612. Standard reference materials used as external standards for laser ablation ICP-MS. SRMs were run between every 6 to 10 analyses on the laser. Data points show the mean of multiple analyses divided by published values (GeoRem): NIST 612 n=22, BHVO-2g n=17, JB sulfide n=13. JB sulfide was used primarily to determine how well the sulfides were ablating, even though it does not contain all the elements of interest. There are no known published values for As, Se, Ag and Tl for BHVO-2G. Error bars are 2σ from replicate analyses. Isotopes chosen for data analysis were Cu 63, Ga 71, Ge 74, As 75, Mo 95, Ag 109, Cd 111, In 115, Sn 119, Sb 121, Tl205, Pb 208, and Bi 209.

Within the sample data, large uncertainties associated with some sample means can reflect true heterogeneity of the glasses, but may also reflect the difficulty in simultaneously measuring multiple extremely low abundance (10-100 ppb) elements by LA-ICP-MS with a limited spot size. True glass heterogeneity can be recognized if an increase in spot size (i.e., an increase in sensitivity for low abundance elements) does not improve the RSD associated with multiple spot analyses on a thin section.

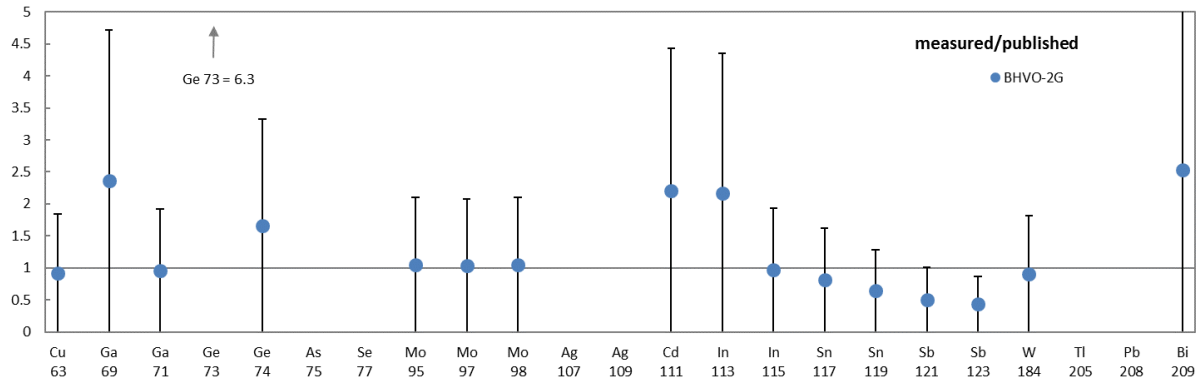

Figure A-BHVO2g. Standard reference materials used as external standards for laser ablation ICP-MS. SRMs were run between every 6 to 10 analyses on the laser. Data points show the mean of multiple analyses divided by published values (GeoRem): NIST 612 n=22, BHVO-2g n=17, JB sulfide n=13. JB sulfide was used primarily to determine how well the sulfides were ablating, even though it does not contain all the elements of interest. There are no known published values for As, Se, Ag and Tl for BHVO-

2G. Error bars are 2σ from replicate analyses. Isotopes chosen for data analysis were Cu 63, Ga 71, Ge 74, As 75, Mo 95, Ag 109, Cd 111, In 115, Sn 119, Sb 121, Tl205, Pb 208, and Bi 209.

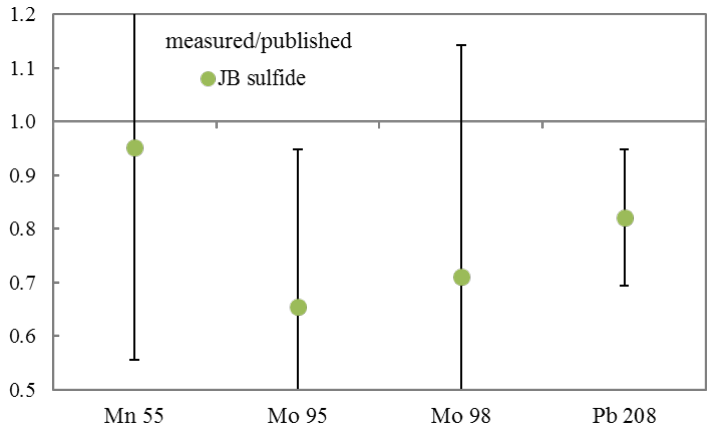

Figure A-JBsulfide. Standard reference materials used as external standards for laser ablation ICP-MS. SRMs were run between every 6 to 10 analyses on the laser. Data points show the mean of multiple analyses divided by published values (GeoRem): NIST 612 n=22, BHVO-2g n=17, JB sulfide n=13. JB sulfide was used primarily to determine how well the sulfides were ablating, even though it does not contain all the elements of interest. There are no known published values for As, Se, Ag and Tl for BHVO-2G. Error bars are 2σ from replicate analyses. Isotopes chosen for data analysis were Cu 63, Ga 71, Ge 74, As 75, Mo 95, Ag 109, Cd 111, In 115, Sn 119, Sb 121, Tl205, Pb 208, and Bi 209.

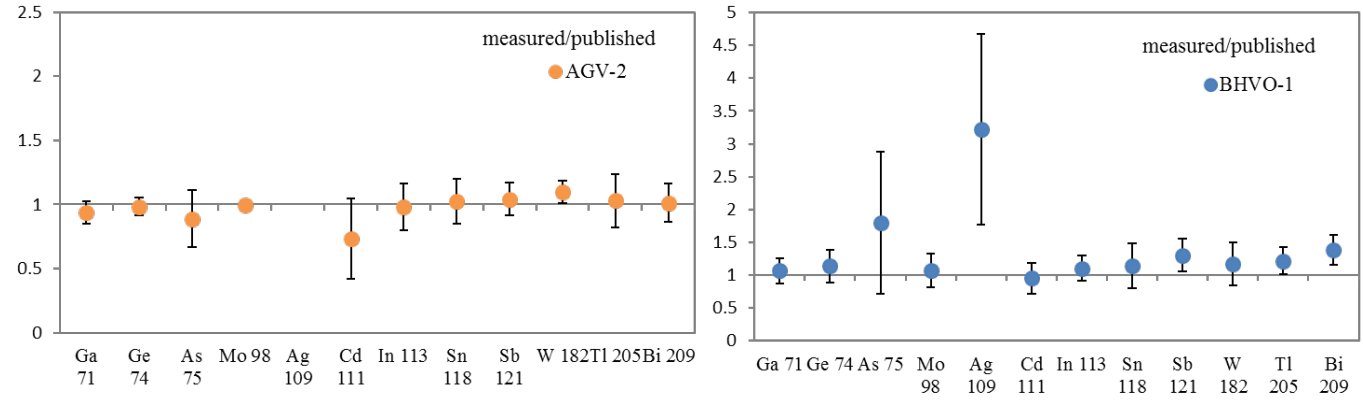

Figure A-standard addition. Standard reference materials used as external standards for standard addition solution ICP-MS. Data points represent the mean of multiple analyses (n~6) normalized to published values (Gaschnig et al., 2014). Arsenic and Ag are normalized to USGS values (no published value for Ag in AGV-2). The isotopes chosen for data analysis are displayed. Error bars represent 2σ.

Greaney et al.
The behavior of chalcophile elements during magmatic differentiation as observed in Kilauea Iki lava lake, Hawaii

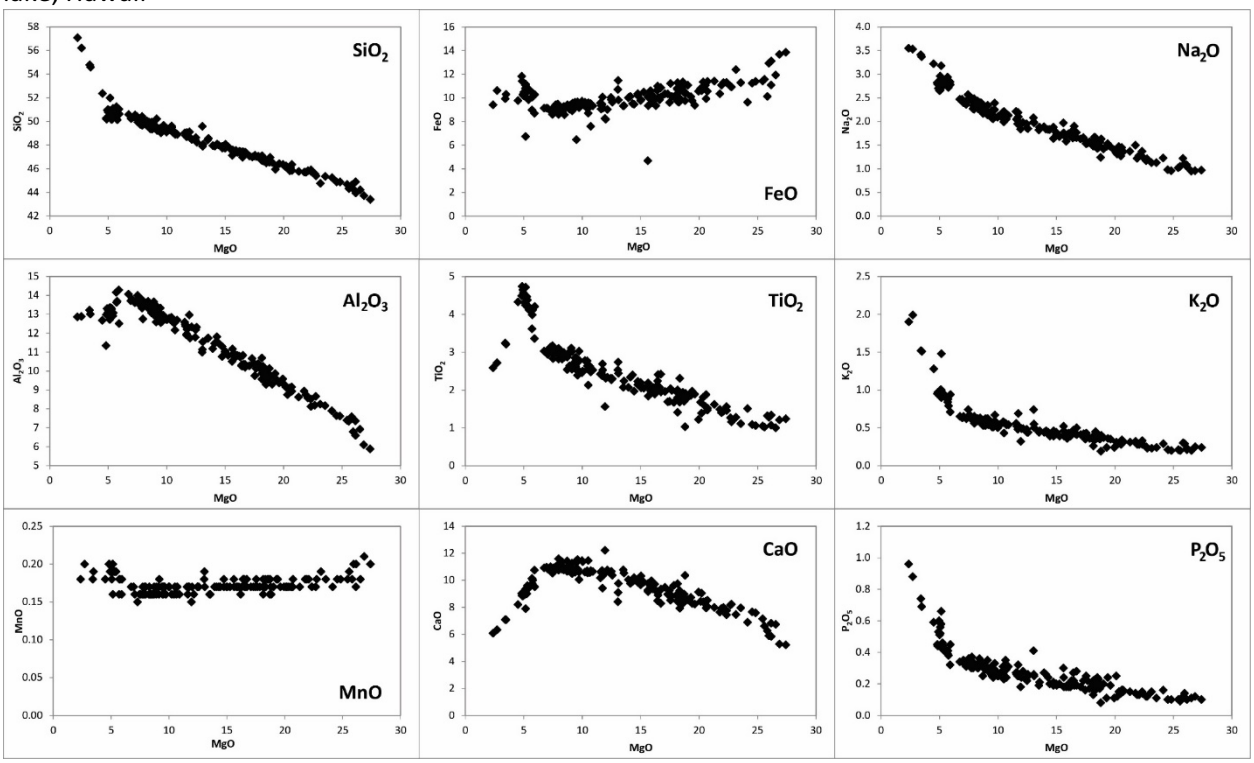

Figure A-WR. Whole rock variation diagrams of major element differentiation trends, data from Helz and Taggert (2010).

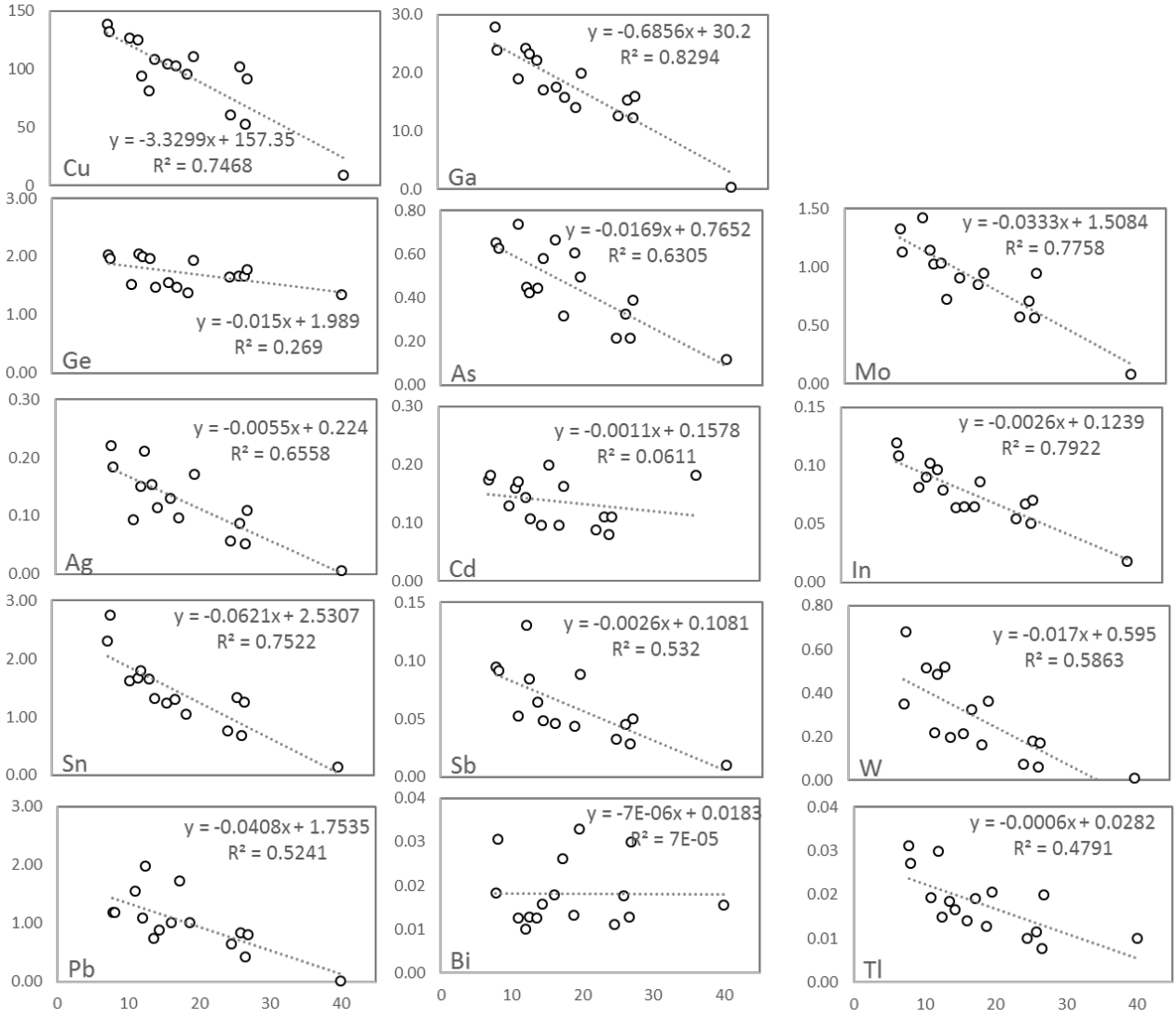

Figure A-regression: Regressions used to calculate the primitive KI composition. Note Cd and Bi R2 are extremely low and caution should be taken when interpreting the Cd and Bi source composition.

Kilauea source composition (batch melting equation)

The regression of Puchtel et al (2004) resulted in an R^2 of >0.5 for all elements except Cd and Bi, so these elements are not well constrained in the Kilauea mantle source.

Bulk partition coefficients for the batch melting equation were calculated using the source modal mineralogy of Norman and Garcia (1999): 65% spinel lherzolite (90% olivine + opx, 10% cpx) and 35% garnet lherzolite (80% olivine +opx, 10% cpx, 10% garnet). We used olivine and clinopyroxene partition coefficients measured in this study, while orthopyroxene and garnet D values were taken from Liu et al. (2014) for Cu, and Salters and Stracke (2004) for Ce and Er, and Adam and Green (2006) for all other elements.

We first modeled a depleted MORB mantle given the average concentrations of Cu, Ga, Ge, As, Mo, Ag, Cd, In, Sn, Sb, La, Er, W, Tl, Pb, and Bi in MORB from Jenner and O'Neill (2012). Again, using the batch melting equation we use bulk D values calculated with the modal mineralogy of Workman and Hart (2005) of 57% olivine, 28% cpx, 13% garnet, and 1.99% spinel with 0.01% sulfide given the low melt fraction of 6% (Workman and Hart, 2005). Then this DMM composition was mixed with between 10 and 20% recycled oceanic crust, of which 95% to 99% is MORB (Jenner and O'Neill, 2012) and UCC sediments compose the remaining 5 to 1%.

Subduction effects on model

Lead, As, Sb, and Tl are predicted to partition into the mantle wedge along with a fluid phase during subduction (Noll et al., 1996), thus depleting these elements from the slab and lowering their contribution to the mantle plume source. Copper and Ag may also be enriched in the mantle wedge from the oxidation of slab sulfides (Timm et al., 2012), suggesting that other chalcophile elements like Cd, In, and Bi may also be released from the slab. There is conflicting evidence as to whether Mo, Sn, and W would be removed from or maintained in the slab (Noll et al., 1996; König et al., 2008; Bali, 2012; Timm et al., 2012), and we are not aware of studies of Ga and Ge in subduction zones. However, depletion of these elements from the slab would not greatly affect the mixing model assuming the elements are mostly removed from terrigenous sediments that may melt or release fluids during subduction. In fact, loss of Pb, As, Tl, and Cu from the slab and sediment package would move the mixing lines (gray region, Fig. 9) closer to that of the estimated KI source.

References

Adam J., and Green T. (2006) Trace element partitioning between mica- and amphibole- bearing garnet lherzolite and hydrous basanitic melt: 1. Experimental results and the investigation of controls on partitioning behavior, *Contrib. Mineral. Petrol.* **152**, 1-17

Helz R.T. and Taggart J.E. Jr. (2010) Whole-Rock Analyses of Core Samples from the 1988 Drilling of Kilauea Iki Lava Lake, Hawaii, *USGS Open-file Report 2010-1093*

Liu X., Xiong X., Audetat A., Li Y., Song M., Li L., Sun W., Ding X. (2014) Partitioning of copper between olivine, orthopyroxene, clinopyroxene, spinel, garnet and silicate melts are upper mantle conditions, *Geochim. Cosmochim. Acta* **125**, 1-22

Norman M.D. and Garcia M.O. (1999) Primitive magmas and source characteristics of the Hawaiian plume: petrology and geochemistry of shield picrites *Earth and Planet. Sci. Lett.* **168**, 27-44

Salters V.J. and Stracke A. (2004) Composition of the depleted mantle, *Geochem. Geophys. Geosyst.* **5**, 1-27

Workman R.K. and Hart S.R. (2005) Major and trace element composition of the depleted MORB mantle (DMM) *Earth and Planet. Sci. Lett.* **231**, 53-72

Bali E., Keppler H., Audetat A. (2012) The mobility of W and Mo in subduction zone fluids and the Mo-W-Th-U systematics of island arc magmas, *Earth and Planet. Sci. Lett.* **315-352**, 195-207

König S., Munker C., Schuth S., Garbe-Schonberg D. (2008) Mobility of tungsten in subduction zones, *Earth and Planet. Sci. Lett.* **274**, 82-92

Noll P.D., Newsom H.E., Leeman W.P., Ryan G. (1996) The role of hydrothermal fluids in the production of subduction zone magmas: Evidence from siderophile and chalcophile trace elements and boron, *Geochim. Cosmochim. Acta* **60**, 587-611

Timm C., Ronde C.E.J., Leybourne M.I., Layton-Matthews D., Graham I.J. (2012) Sources of chalcophile and siderophile elements in Kermadec arc magmas, *Econ. Geol.* **107**, 1527-1238